



**NAVAL  
POSTGRADUATE  
SCHOOL**

**MONTEREY, CALIFORNIA**

**THESIS**

**TRANSIENT HEAT TRANSFER PROPERTIES IN A PULSE  
DETONATION COMBUSTOR**

by

Dion G. Fontenot

March 2011

Thesis Advisor:  
Second Reader:

Christopher M. Brophy  
Knox T. Millsaps

**Approved for public release; distribution is unlimited**

THIS PAGE INTENTIONALLY LEFT BLANK

<b>REPORT DOCUMENTATION PAGE</b>			<i>Form Approved OMB No. 0704-0188</i>
Public reporting burden for this collection of information is estimated to average 1 hour per response, including the time for reviewing instruction, searching existing data sources, gathering and maintaining the data needed, and completing and reviewing the collection of information. Send comments regarding this burden estimate or any other aspect of this collection of information, including suggestions for reducing this burden, to Washington headquarters Services, Directorate for Information Operations and Reports, 1215 Jefferson Davis Highway, Suite 1204, Arlington, VA 22202-4302, and to the Office of Management and Budget, Paperwork Reduction Project (0704-0188) Washington DC 20503.			
<b>1. AGENCY USE ONLY (Leave blank)</b>	<b>2. REPORT DATE</b> March 2011	<b>3. REPORT TYPE AND DATES COVERED</b> Master's Thesis	
<b>4. TITLE AND SUBTITLE</b> Transient Heat Transfer Properties in a Pulse Detonation Combustor		<b>5. FUNDING NUMBERS</b>	
<b>6. AUTHOR(S)</b> Dion Glenn Fontenot		<b>8. PERFORMING ORGANIZATION REPORT NUMBER</b>	
<b>7. PERFORMING ORGANIZATION NAME(S) AND ADDRESS(ES)</b> Naval Postgraduate School Monterey, CA 93943-5000		<b>10. SPONSORING/MONITORING AGENCY REPORT NUMBER</b>	
<b>9. SPONSORING /MONITORING AGENCY NAME(S) AND ADDRESS(ES)</b> N/A		<b>11. SUPPLEMENTARY NOTES</b> The views expressed in this thesis are those of the author and do not reflect the official policy or position of the Department of Defense or the U.S. Government. IRB Protocol number ____N/A____.	
<b>12a. DISTRIBUTION / AVAILABILITY STATEMENT</b> Approved for public release; distribution is unlimited		<b>12b. DISTRIBUTION CODE</b>	
<b>13. ABSTRACT (maximum 200 words)</b>  The heat transfer along the axis of a pulse detonation combustor has been characterized for various frequencies and fill fractions at 2.5 atmospheres of pressure for chamber refresh conditions. In a pulse detonation combustor, a supersonic detonation wave is the method for transforming chemical energy into mechanical energy and the wave propagates much faster than the subsonic flames in devices such as rockets and ramjets. The flow field inside a pulse detonation combustor is highly turbulent, unsteady, and varies largely during each combustion cycle. By determining the heat transfer properties at multiple axial locations and the associated combustor wall temperatures, proper combustor material selection can ensure the material properties will not deteriorate and therefore allow for practical operational lifetimes. Experimental testing measured the axial heat transfer characteristics in a pulse detonation combustor at various operating conditions and multiple cooling jacket locations. Computer simulations were used to model the heat transfer inside the pulse detonation combustor and correlate those predications with empirical data. The acquired data from the comparison of the computer simulations and the experimental results was correlated and demonstrated good agreement. The determined values should allow designers the ability to consider regenerative fueling strategies for future systems.			
<b>14. SUBJECT TERMS</b> Pulse Detonation Engines, PDE, Heat Transfer		<b>15. NUMBER OF PAGES</b> 89	
		<b>16. PRICE CODE</b>	
<b>17. SECURITY CLASSIFICATION OF REPORT</b> Unclassified	<b>18. SECURITY CLASSIFICATION OF THIS PAGE</b> Unclassified	<b>19. SECURITY CLASSIFICATION OF ABSTRACT</b> Unclassified	<b>20. LIMITATION OF ABSTRACT</b> UU

THIS PAGE INTENTIONALLY LEFT BLANK

**Approved for public release; distribution is unlimited**

**TRANSIENT HEAT TRANSFER PROPERTIES IN A PULSE DETONATION  
COMBUSTOR**

Dion G. Fontenot  
Lieutenant, United States Navy  
B.S., North Carolina State University, 2004

Submitted in partial fulfillment of the  
requirements for the degree of

**MASTER OF SCIENCE IN MECHANICAL ENGINEERING**

from the

**NAVAL POSTGRADUATE SCHOOL  
March 2011**

Author: Dion G. Fontenot

Approved by: Christopher M. Brophy  
Thesis Advisor

Knox T. Millsaps  
Second Reader

Knox T. Millsaps  
Chair, Department of Mechanical and Aerospace Engineering

THIS PAGE INTENTIONALLY LEFT BLANK

## **ABSTRACT**

The heat transfer along the axis of a pulse detonation combustor has been characterized for various frequencies and fill fractions at 2.5 atmospheres of pressure for chamber refresh conditions. In a pulse detonation combustor, a supersonic detonation wave is the method for transforming chemical energy into mechanical energy and the wave propagates much faster than the subsonic flames in devices such as rockets and ramjets. The flow field inside a pulse detonation combustor is highly turbulent, unsteady, and varies largely during each combustion cycle. By determining the heat transfer properties at multiple axial locations and the associated combustor wall temperatures, proper combustor material selection can ensure the material properties will not deteriorate and therefore allow for practical operational lifetimes. Experimental testing measured the axial heat transfer characteristics in a pulse detonation combustor at various operating conditions and multiple cooling jacket locations. Computer simulations were used to model the heat transfer inside the pulse detonation combustor and correlate those predications with empirical data. The acquired data from the comparison of the computer simulations and the experimental results was correlated and demonstrated good agreement. The determined values should allow designers the ability to consider regenerative fueling strategies for future systems.

THIS PAGE INTENTIONALLY LEFT BLANK

# TABLE OF CONTENTS

I.	INTRODUCTION.....	1
II.	BACKGROUND .....	5
A.	DESCRIPTION OF BASIC PULSE DETONATION ENGINE OPERATION .....	5
B.	COMBUSTION PROCESSES .....	6
1.	Deflagration .....	6
2.	Detonation.....	6
C.	HEAT TRANSFER OF THE COMBUSTION CHAMBER.....	7
1.	Conduction Through the Combustor/Cooling Jacket Wall.....	8
2.	Convection Along the Cooling Jacket Inner Wall .....	9
a.	<i>Velocity Boundary Layer</i> .....	10
b.	<i>Thermal Boundary Layer</i> .....	12
c.	<i>Fully Developed Internal Flow</i> .....	12
3.	Convection Along the Combustor Inner Wall.....	15
III.	DESIGN AND EXPERIMENTAL SETUP .....	17
A.	PULSE DETONATION ENGINE.....	17
B.	FUEL AND AIR DELIVERY .....	18
1.	Air.....	18
2.	Ethylene .....	18
3.	Ignition System.....	20
C.	COMBUSTOR ASSEMBLY .....	22
1.	Combustor .....	22
2.	Cooling Jackets.....	24
3.	Cooled Nozzle .....	25
4.	Cooling Water System .....	25
D.	INSTRUMENTATION .....	27
1.	Thermocouples .....	27
2.	Pressure Transducers .....	28
3.	Kistler Pressure Sensors.....	28
E.	DATA ACQUISITION.....	30
F.	PDE CONTROLLER AND OPERATING PROCEDURE .....	31
G.	COOLING WATER MASS FLOWRATE.....	32
H.	PRESSURE TRANSDUCER CALIBRATION .....	34
IV.	EXPERIMENTAL RESULTS.....	35
A.	TESTING AT 20 HZ .....	35
B.	TESTING AT 30 HZ .....	38
C.	COMPARISONS OF 20HZ AND 30 HZ TESTING .....	42
D.	COMPARISONS OF 30 HZ AND 40 HZ TESTING .....	45
E.	COMPUTATIONAL FLUID DYNAMICS MODELING .....	46
F.	UNCERTAINTY ANALYSIS.....	52

<b>V.</b>	<b>CONCLUSIONS AND FUTURE WORK</b> .....	<b>55</b>
<b>A.</b>	<b>CONCLUSIONS</b> .....	<b>55</b>
<b>B.</b>	<b>FUTURE WORK</b> .....	<b>56</b>
	<b>APPENDIX A: PDE STANDARD OPERATING PROCEDURES</b> .....	<b>57</b>
	<b>APPENDIX B: COOLING WATER SYSTEM</b> .....	<b>61</b>
	<b>APPENDIX C: COMBUSTOR ASSEMBLY DRAWINGS</b> .....	<b>63</b>
	<b>LIST OF REFERENCES</b> .....	<b>69</b>
	<b>INITIAL DISTRIBUTION LIST</b> .....	<b>71</b>

## LIST OF FIGURES

Figure 1.	Comparison of High-Speed Propulsion Technologies (From [1]).....	2
Figure 2.	Simplified Ideal PDE Operation Cycle (After [4]) .....	5
Figure 3.	Heat transfer through a plane wall (After [9]) .....	8
Figure 4.	Velocity Boundary Layer Development on a Flat Plate (From [7]) .....	11
Figure 5.	Variation of Velocity Boundary Layer Thickness $\delta$ and the Local Heat Transfer Coefficient $h$ for Flow Over an Isothermal Flat Plate (From [7]) .....	11
Figure 6.	Thermal Boundary Layer Development on an Isothermal Flat Plate (From [7]).....	12
Figure 7.	Laminar, Hydrodynamic Boundary Layer Development in a Circular Tube (From [7]).....	13
Figure 8.	Thermal Boundary Layer Development in a Heated Circular Tube (From [7]).....	16
Figure 9.	Naval Postgraduate School Rocket Propulsion Laboratory Test Cell #2 .....	17
Figure 10.	Test Cell 2 Fuel and Gas Tanks .....	19
Figure 11.	PDE Fuel Arms and Injectors .....	20
Figure 12.	Flow Path for Transient Plasma Ignition (From [6]) .....	21
Figure 13.	TPI Electrode Shroud.....	21
Figure 14.	PDE Combustor .....	22
Figure 15.	Dvorak Swept-Tall Ramp (From [6]) .....	23
Figure 16.	Swept Ramp Configuration Inside Combustor [From (8)] .....	23
Figure 17.	PDE Cooling Jacket .....	24
Figure 18.	Cooling Water Tank (Left) and Regenerative Turbine Water Pump (Right) (From [8]).....	25
Figure 19.	PDE Cooling Water Supply and Discharge Manifolds.....	26
Figure 20.	Kistler Pressure Sensor and Kistler Cooling Jacket (From [8]).....	29
Figure 21.	Kistler Amplifiers .....	29
Figure 22.	National Instruments LabView Data Acquisition System .....	30
Figure 23.	National Instruments LabView Test Cell #2 PDE Controller 1 .....	31
Figure 24.	LabView Interface Controller (From [8]) .....	32
Figure 25.	Calibration of Pressure Transducers .....	34
Figure 26.	Heat Transfer Rates for 20 Hz Tests.....	36
Figure 27.	Combustor Wall Temperatures for 20 Hz Tests .....	37
Figure 28.	Combustor Temperature Profiles for 20 Hz Tests .....	38
Figure 29.	Heat Transfer Rates for 30 Hz Testing .....	40
Figure 30.	Heat Transfer Rate Profiles for 30 Hz Tests.....	41
Figure 31.	Combustor Wall Temperatures at CW7 for Fuel Fill Times of 14–18 ms .....	42
Figure 32.	Combustor Wall Temperature Comparisons at 20 Hz and 30 Hz .....	43
Figure 33.	Temperature Profile Comparisons at 20 Hz and 30 Hz .....	44
Figure 34.	Combustor Wall Temperature Comparisons at CW7 for 20 Hz and 30 Hz .....	45
Figure 35.	Combustor Wall Temperatures at CW7 for 30 and 40 Hz Tests .....	46
Figure 36.	CFD Temperature Profiles for Detonation .....	48
Figure 37.	Temperature and Pressure Profile in a Detonation Wave (0.250 ms).....	49

Figure 38.	Temperature Profile in a Detonation Wave (1.250 ms).....	50
Figure 39.	Temperature Profile in a Detonation Wave (1.750 ms).....	51
Figure 40.	Cooling Water System Schematic .....	61
Figure 41.	Combustor Section – Isometric View (From [8]).....	63
Figure 42.	Combustor Sections – Plan View (From [8]) .....	64
Figure 43.	Combustor Sections – Inner Tube (From [8]).....	65
Figure 44.	Cooling Nozzle – Inner Tube (From [8]).....	66
Figure 45.	Cooling Nozzle – Assembly (From [8]) .....	67

## LIST OF TABLES

Table 1.	Thermocouple Connections .....	27
Table 2.	Pressure Transducer Connections .....	28
Table 3.	Various Cooling Water Mass Flow Rates.....	33
Table 4.	Pressure Transducer Calibrations .....	34

THIS PAGE INTENTIONALLY LEFT BLANK

## LIST OF ACRONYMS AND ABBREVIATIONS

CFD	Computational Fluid Dynamic	
CW	Cooling Water	
DDT	Deflagration-to-Detonation Transition	
GPM	Gallons per Minute	
GUI	Graphical User Interface	
NPS	Naval Postgraduate School	
PDC	Pulse Detonation Combustion	
PDE	Pulse Detonation Engine	
RPL	Rocket Propulsion Laboratory	
RTV	Room Temperature Vulcanizing	
TPI	Transient Plasma Ignition	
A	Area	[ <i>m</i> ]
atm	Atmospheres	
C	Celsius	
cm	centimeter	
$c_p$	Specific heat capacity	[ <i>kJ/kg · K</i> ]
D	Diameter	[ <i>m</i> ]
$D_h$	Hydraulic diameter	[ <i>m</i> ]
$F/A$	Fuel air ratio	
$h$	Heat transfer coefficient	[ <i>W/m<sup>2</sup> K</i> ]
$\bar{h}$	Average heat transfer coefficient	[ <i>W/m<sup>2</sup> K</i> ]
Hz	Hertz	[ <i>sec<sup>-1</sup></i> ]
$I_{sp}$	Specific impulse	[ <i>sec</i> ]
$k$	Thermal conductivity	[ <i>W/m · K</i> ]
K	Kelvin	
L	Length	[ <i>m</i> ]
m	Meter	

$\dot{m}$	Mass flow rate	$[kg/s]$
ms	Milliseconds	
Nu	Nusselt number	
$q$	Heat flux	$[W/m^2]$
$q''$	Heat transfer rate	$[W]$
P	Wetted perimeter	$[m]$
Pa	Pascal	
Re	Reynolds number	
$T_{g,wall}$	Temperature of the combustor inner wall	$[^{\circ}C]$
$T_{l,wall}$	Temperature of the inner jacket wall	$[^{\circ}C]$
$T_{m,in}$	Mean temperature in	$[^{\circ}C]$
$T_{m,out}$	Mean temperature out	$[^{\circ}C]$
$\varphi$	Phi	
$\rho$	Density	$[kg/m^3]$
$\mu$	Viscosity	$[kg/m \cdot s]$

## ACKNOWLEDGMENTS

I would like to thank my thesis advisor Dr. Christopher Brophy for giving me the opportunity to work at the Rocket Propulsion Laboratory on the Pulse Detonation Engine. His knowledge, support and direction provided an invaluable learning experience.

I would also like to thank Mr. Dave Dausen for teaching me how operate all of the software associated with this work. Thanks for sharing your technical knowledge as well as your friendship and positive outlook.

Mr. George Hageman thanks for always lending hand in any work from the test cell to the control room. While you are around, things are guaranteed to never be dull.

Thanks to Bobby Wright for your assistance and technical knowledge throughout the PDE testing.

Finally, I would like to express my appreciation to my wife Shelly, and my sons Cody, Brandon, and Tyler for their encouragement, support, and understanding during this challenging time.

THIS PAGE INTENTIONALLY LEFT BLANK

## I. INTRODUCTION

Pulse detonation combustion (PDC) is a technology in which there has been much research and growing interest in the last several years. This technology is still in the developmental stages, and is demonstrating the ability to produce improved performance over many proven sources of propulsion and power generation. Technical challenges associated with PDC systems are being overcome and are revealing the potential advantages over current technologies. If applied to flight, pulse detonation combustion can be used to power a tactical missile with a Pulse Detonation Engine (PDE) and provide greater range for the same amount of fuel as compared to other current technologies.

As advances continue in material sciences, the PDE could see a wider operational range at higher flight Mach numbers by using lighter and stronger materials that could withstand higher operating temperatures and conditions within the combustor. With significant improvements in thermal efficiency and simplicity of design as compared to other types of engines, PDEs could make an excellent propulsion source for supersonic tactical missile designs.

As seen in Figure 1, the specific impulse,  $I_{sp}$ , or fuel efficiency, of a PDE is greater than ramjets, scramjets, ducted rockets and solid rockets. The upper band of a turbojet represents fuel-lean operation and exceeds a PDE in specific impulse. The PDE performance could, therefore, be improved substantially if operated fuel-lean or under partial fill conditions. A PDE, however, is constructed with very few moving parts as compared to a turbojet, therefore greatly reducing costs associated with production and construction.

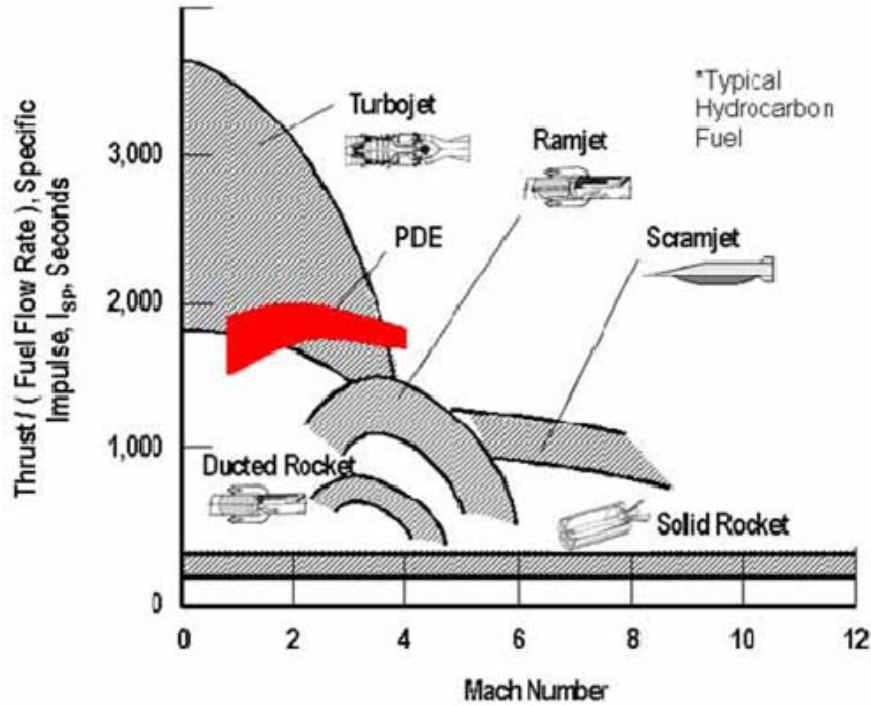


Figure 1. Comparison of High-Speed Propulsion Technologies (From [1])

Further research is also ongoing in using hybrid PDC gas turbine systems for power generation applications. Gas turbines are known for great overall efficiencies but often only while operating at design conditions, which are where most U.S. naval ships do not spend extensive time operating. Gas turbines lose their great efficiency when operating at lower speeds, while ships are patrolling or while in port at idle settings. By using a hybrid PDE gas turbine system, an efficient PDC could improve performance at lower rotational speeds, therefore increasing the overall system efficiency during low and high power demand operations.

In order to achieve improved performance in detonation-based systems, a full understanding of the thermal loads experienced by a PDC is essential for developing their practical use. In a PDC, the combustor is operated in a cyclical manner by producing multiple detonation waves per second. These detonation waves create substantial transient chamber pressures at high operating temperatures. The extremely transient and

brutal environment makes it especially difficult to experimentally obtain time resolved heat transfer measurements and few studies have been published in this area.

This becomes a challenging problem to solve, which requires comprehension of fluid dynamics and heat transfer of turbulent flow. The turbulence created in the combustor creates random fluctuations in the fluid and on both a global and a local scale the flow becomes highly unsteady. Hence, a time averaged value may be used in order to achieve a parameter that is independent of time and assumed to be quasi steady. Naples, Hoke, and Schauer [2] at the Air Force Research Laboratory performed an experiment that studied the heat loads from steady deflagration and pulsed detonation combustion by placing a cross flow tube within the flow field of the combustor in order to measure the time averaged heat transfer. The unsteady flow of a PDE cycle develops an environment that is thermally different from that of a continuous flow cycle. The results displayed a 20–30% lower heat load in pulse detonation as compared to steady deflagration. The experiment also revealed that the un-insulated combustor wall temperature for steady state deflagration was in excess of 1,400°F while the pulse detonation cycle resulted in an approximate temperature of 1,050°F. Concluding, the violent combustion of pulse detonation transferred less heat to the wetted surface area than a steady deflagration combustor setup.

At the NASA Glenn Research Center, Paxson [3] conducted research by comparing experimentally measured and numerically simulated, time-averaged, point heat transfer rates in a PDE using a cylinder in cross-flow and a spool design. The cross-flow cylinder was placed directly in the combustion gas flow field, which produces different results as compared to the heat transfer occurring through the combustor wall. The computational fluid dynamics (CFD) model was validated by agreement with measured and computed results of several locations under different operating conditions. These results were completed on an open-ended combustion chamber that allowed flow reversals from the atmosphere to enter the combustion chamber, which provided cooling that could not be accurately accounted for.

Further research is needed to characterize the changes in heat transfer rates along the length of the combustor without introducing any obstacles into the already

complicated flow field and with a nozzle ended combustion chamber to prevent flow reversals. These results would lead to time-averaged values for an effective heat transfer coefficient of the combustor. Ultimately, it is desirable to obtain local parameters at the combustor wall vs. time-averaged values.

The objective of this research is to characterize the heat transfer properties along the axis of a PDC for various frequencies and fill fractions. Experimental testing was performed to determine the heat transfer characteristics at multiple axial combustor locations for operations at 20, 30 and 40 Hz with varying fill fractions of 14, 16, and 18 milliseconds. Experimental testing contributed in determining the regions of highest heat transfer and hence where the greatest amount of cooling is required. Computational fluid dynamics modeling was used to model the heat transfer inside a combustor during a pulse detonation event, and correlated with empirical data.

## II. BACKGROUND

### A. DESCRIPTION OF BASIC PULSE DETONATION ENGINE OPERATION

A prototypical, straight -tube, valve-less PDC is closed at one end and opens at the other end. In some cases, a nozzle may or may not be included as part of the PDC. The various stages of the pulse detonation combustion cycle consist of four basic steps: detonation, blow down, purge and fill. Figure 2 displays the basic combustion cycle of a PDE and give a visual understanding of the events that are occurring during a cycle.

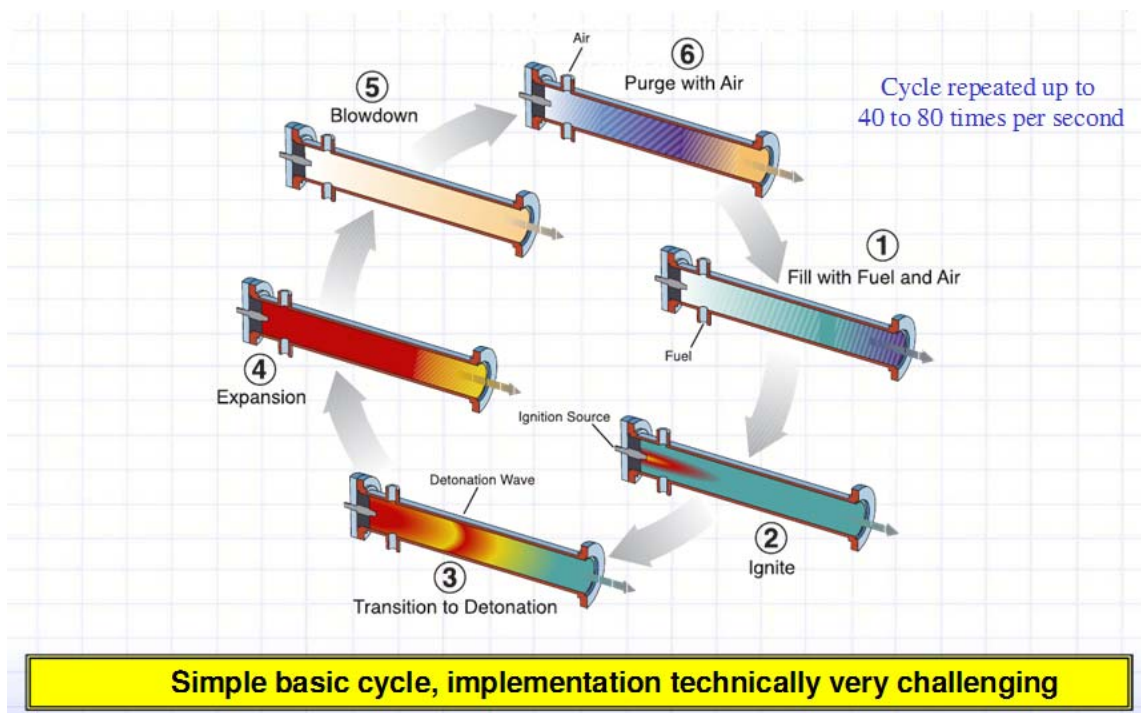


Figure 2. Simplified Ideal PDE Operation Cycle (After [4])

In the first step during the fill stage, the cycle is prepared by injecting a mixture of fuel and oxidizer into the head end of the combustor. In step two, the mixture is ignited, which creates a deflagration event in the combustion chamber. Steps three and four displays the resulting flame that travels some distance and then experiences deflagration-to-detonation transition (DDT). The detonation wave travels down the combustor and

exits to the atmosphere. Blow down starts to occur in step five after the detonation wave exits the tube and expansion waves move upstream towards the end-wall. Once these expansion waves reach the end-wall, the pressure in the chamber begins to drop while still producing a decreasing thrust. In the final step, the end-wall pressure has dropped low enough to allow purge gases to flow into the combustion chamber. During the purge stage, a slug of purge gas is typically injected to isolate the combustion products from the next fill and then a new cycle begins.

## **B. COMBUSTION PROCESSES**

### **1. Deflagration**

The most common type of combustion process is the deflagration combustion process that exists in majority of engines in use today. The majority of all flight engines and ground-based power generation systems burn fuel as a deflagration to release the energy contained within the fuel. During the deflagration process, combustion is occurring at subsonic velocities. This process occurs at nearly constant-pressure conditions. The combustion wave propagates down the combustor and energy is transferred to the working fluid via thermal diffusion. Deflagration combustion can be a continuous process such a burning open flame.

### **2. Detonation**

The combustion process of a PDE transitions from a deflagration combustion process to detonation combustion. Understanding the detonation process is essential in evaluating the heat transfer process of the combustion chamber. Detonation occurs at supersonic combustion wave speeds during a constant volume process. A fuel/air mixture traveling at a subsonic velocity is compressed by a normal shock wave propagating at a high Mach number, which is then followed by a rapid release of heat and a sudden rise in pressure. The coupling of a strong shock to a region of heat release is

called a detonation. This is a very violent, rapid, exothermic reaction, which produces a harsh environment in which it is difficult to experimentally document the instantaneous changes in local pressures and temperatures.

The detonation process results in pressure gains across the combustion wave where a deflagration combustion process results in a minimal or no pressure rise. Also through detonation, combustion products exhibit higher temperatures due to the inherent compression and less dissociation. A deflagration will often occur as a lower flame temperature and the process is typically continuous. During detonation, the higher flame temperatures are only periodic from the nature of the cycle. The fill and purge steps result in a cooling portion of the cycle.

Detonation of a fuel/air mixture is often difficult to initiate within a short length combustor. One method to achieve detonation is to start with deflagration combustion and then transition the flame front to a detonation to by inserting obstacles in the flow field. The obstacle causes the flow to speed up as well as creating turbulent mixing. This results in a process known as Deflagration to Detonation Transition (DDT). A common obstacle used in the flow field is a Shchelkin spiral, but this causes a noticeable pressure loss during the filling and detonation portion of the cycle [5]. A more recent study by Dvorak [6] demonstrates that using obstacles such as swept ramps can provide at least a 27% improvement over the total pressure loss of a wall spiral with the same DDT performance.

### **C. HEAT TRANSFER OF THE COMBUSTION CHAMBER**

Extended operation of a PDC at practical frequencies and pressures requires cooling of the combustor wall. A water cooling system is currently in use at the Naval Postgraduate School Rocket Propulsion Laboratory to ensure overheating and failure of the combustor wall does not occur and allows overall heat transfer values to be determined for future design purposes. Heat is transferred from the bulk of the combustion gases in the combustion chamber to the combustor wall surface via forced convection. From there, the heat flows through the combustor wall to inner wall of the

cooling jacket by means of conduction. Finally, forced convection occurs as the cooling water bulk fluid transports heat away from the surface of the cooling jacket inner wall.

### 1. Conduction Through the Combustor/Cooling Jacket Wall

Heat is transferred by conduction through the combustor wall under the assumed one-dimensional, steady state conditions. Heat transfer is occurring all the way through the wall without any internal generation of thermal energy. As shown in Figure 3, heat is transferred in the  $x$  direction and temperature is a function of  $x$ . The combustor wall is physically separating the hot combustor gases from the cold cooling water. Heat transfer occurs from the hot gas through the wall to the cold liquid. If both the gas wall and liquid wall temperatures are known, the conduction heat transfer rate can be determined, as well as a temperature distribution. The inherently unsteady conditions of the detonation process is the driving force for heat transfer to occur across the combustor wall to a quasi steady state process of convection provided by the cooling water side of the combustor wall.

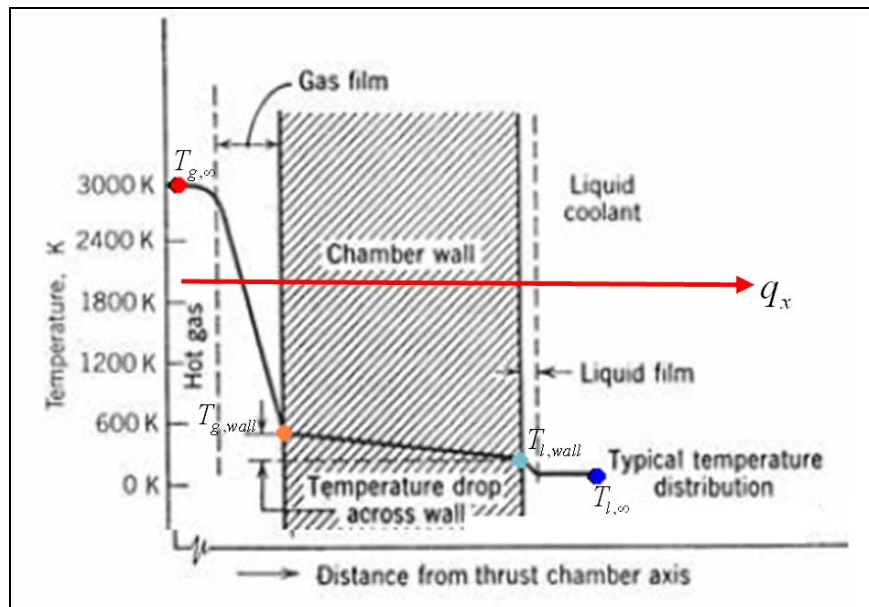


Figure 3. Heat transfer through a plane wall (After [9])

$$\frac{d}{dx} \left( k \frac{dT}{dx} \right) = 0 \quad (1)$$

For a one-dimensional, steady state conduction in a plane wall with no heat generation and a constant thermal conductivity, the temperature through the wall will vary linearly as  $x$  increases [5]. The conduction heat transfer rate,  $q_x$ , and heat flux,  $q_x''$ , through a plane wall is given by Equation (2) and (3).

$$q_x = \frac{kA}{L} (T_{g,wall} - T_{l,wall}) \quad (2)$$

$$q_x'' = \frac{q_x}{A} = \frac{k}{L} (T_{g,wall} - T_{l,wall}) \quad (3)$$

The wall area normal to the direction of heat transfer is noted as the cross-sectional area,  $A$ . The combustor wall is made for 4340 steel that has a thermal conductivity,  $k$ , of 44.5 W/m-K at 300 K. The temperature of the combustor inner wall  $T_{g,wall}$ , is extremely difficult to experimentally measure due to the high pressure, temperatures and transient environment. The small clearances in the cooling jacket make it difficult to measure the liquid side of the inner jacket wall temperature  $T_{l,wall}$ , so an energy balance with the cooling water is required in order to determine the inner wall cooling jacket temperature.

## 2. Convection Along the Cooling Jacket Inner Wall

The primary heat transfer between a surface and a fluid moving over the surface is known as convection. For a transfer of energy to occur, the fluid that may exist as a liquid or a gas moves at a prescribed velocity and there exists a temperature difference between the temperature of the surface and the temperature of the moving fluid. The local heat flux,  $q''$ , is expressed in Equation (4).

$$q'' = \frac{q}{A} = h(T_{wall} - T_{\infty}) \quad (4)$$

The local convection coefficient,  $h$ , will vary on a surface as the flow conditions vary from point to point. This variation in the local convection coefficient will cause the local heat to fluctuate across the surface as well. By using an average convection coefficient,  $\bar{h}$ , for the whole surface, then the total heat transfer rate,  $q$ , can be expressed by Equation (5).

$$q = \bar{h}A_s(T_s - T_\infty) \quad (5)$$

Determination of the local and average convection coefficients is not an easy problem. The coefficients depend on several fluid properties such as density, viscosity, thermal conductivity and specific heat, as well as the flow conditions and surface geometries [7].

*a. Velocity Boundary Layer*

Figure 4 illustrates the flow over a flat plate. The wall surface where the fluid particles make contact, the fluid velocity is assumed to be zero and is often referred to as a no-slip condition. These near-zero velocity particles hinder the fluid layer that is adjacent to the wall. This hindrance between layers continues some distance away from the wall resulting in layers of shear stresses until the distance from the wall increases to a value where the velocity of the fluid changes to that of the free stream. To properly solve a convection problem, it must be determined whether the boundary layer is laminar or turbulent. The laminar boundary layer fluid motion is ordered and in the same direction. The turbulent boundary layer grows larger than the laminar boundary layer and is erratic with fluctuations in all directions.

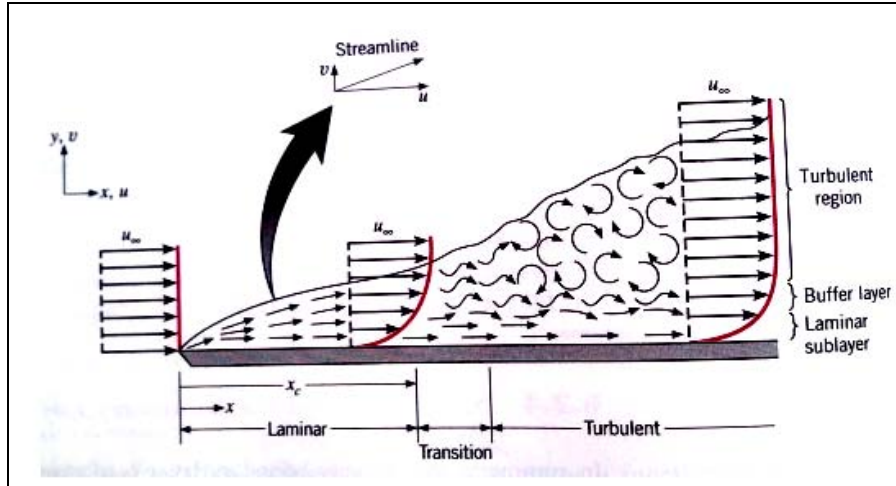


Figure 4. Velocity Boundary Layer Development on a Flat Plate (From [7])

As the boundary transitions from laminar to turbulent, the boundary layer grows larger, while the shear stress and local heat transfer coefficient significantly increase. Notice in Figure 5 the sudden increase in the local heat transfer coefficient as flow transitions from laminar to turbulent.

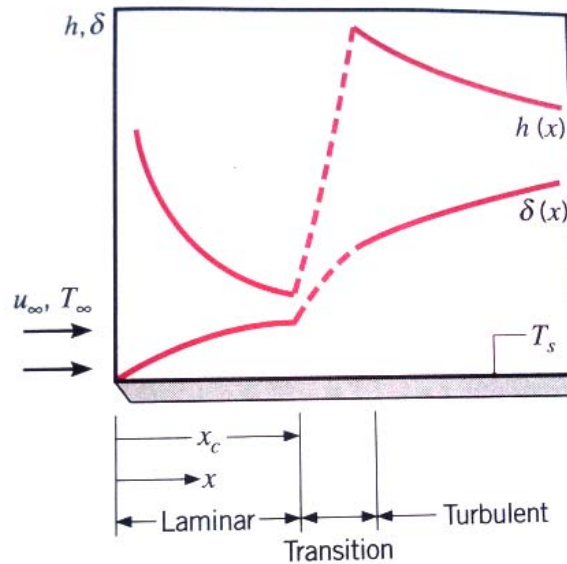


Figure 5. Variation of Velocity Boundary Layer Thickness  $\delta$  and the Local Heat Transfer Coefficient  $h$  for Flow Over an Isothermal Flat Plate (From [7])

**b. Thermal Boundary Layer**

Similar to the growth of a velocity boundary layer, a thermal boundary develops as long as there is a difference in the plate surface temperature and the free stream fluid temperature. Thermal equilibrium is achieved at the wall surface between the wall and the zero velocity particles. At this location, energy transfer only occurs by conduction since there is zero fluid motion. Energy is then transferred by convection from the stationary particles to the adjacent particle in the moving fluid layer and continues to transfer through layers. The growth of the thermal boundary layer is illustrated in Figure 6. The rate of heat transfer is determined by the conditions in the thermal boundary layer and influences the heat flux and the local convective heat transfer coefficient.

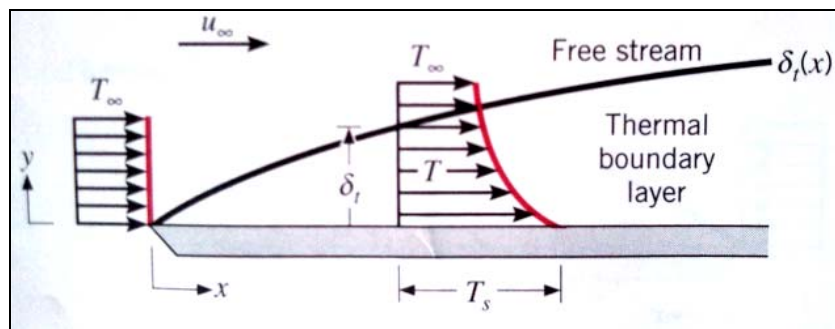


Figure 6. Thermal Boundary Layer Development on an Isothermal Flat Plate  
(From [7])

**c. Fully Developed Internal Flow**

In internal flow, the fluid is confined by a surface; therefore, boundary layer development is limited due to this constraint. The point at which the velocity profile no longer changes is then considered fully developed. For flow through the cooling jacket channels, it must be determined whether the flow is laminar or turbulent in order to establish at which point flow is fully developed. For internal flow, the commencement of turbulence begins at a Reynolds number of approximately 2300, while numbers as large as 10,000 are needed in order to reach fully turbulent conditions. For a circular tube, the Reynolds number can be determined from Equation (6).

$$\text{Re}_D \equiv \frac{\rho u_m D}{\mu} \quad (6)$$

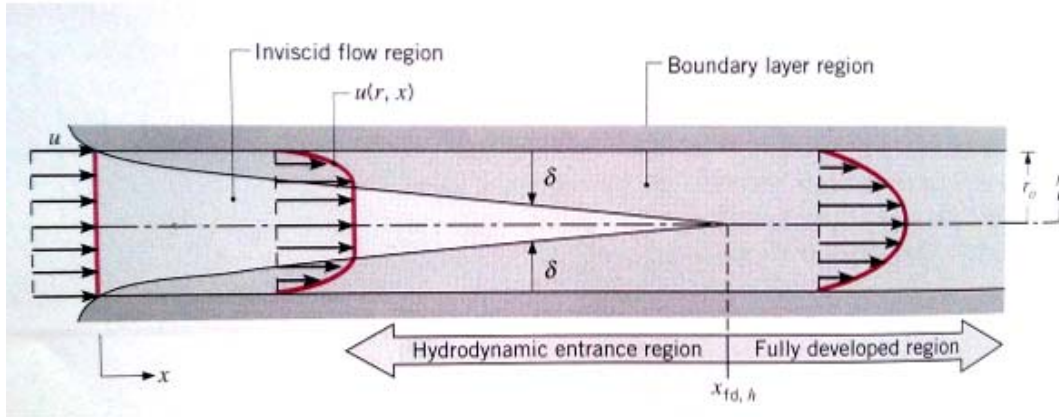


Figure 7. Laminar, Hydrodynamic Boundary Layer Development in a Circular Tube (From [7])

Since there is a variation in the velocity through the cross section of the pipe, the mean velocity,  $u_m$ , is used to solve problem with internal flows. Mass flow rate can then be determined from the mean velocity, density and cross-sectional area as in Equation (7).

$$\dot{m} = \rho u_m A_c \quad (7)$$

For a circular tube with incompressible flow with a constant mass flow rate, the Reynolds number is equivalent to Equation (8). The Reynolds number is interpreted as the ratio of the inertia and viscous forces.

$$\text{Re}_D = \frac{4\dot{m}}{\pi D \mu} \quad (8)$$

Since the cooling jacket water flow channels are square, noncircular tubes use an effective diameter known as the hydraulic diameter, shown in Equation (9). For the cooling jackets, the hydraulic diameter is to be used in calculations for Reynolds and Nusselt numbers. In Equation (9),  $P$  is the wetted perimeter.

$$D_h = \frac{4A_c}{P} \quad (9)$$

The Prandtl number is required to calculate the Nusselt number. The Prandtl number is interpreted as the ratio of momentum and thermal diffusivities.

$$\text{Pr} = \frac{c_p \mu}{k} \quad (10)$$

The Nusselt number can be determined from the Dittus-Boelter equation with the limitations listed below. The Nusselt number is a dimensionless temperature gradient of the surface.

$$Nu_D = 0.023 \text{Re}_D^{4/5} \text{Pr}^n \quad (11) \quad (\text{From [7]})$$

$$\left[ \begin{array}{l} 0.7 \leq \text{Pr} \leq 160 \\ \text{Re}_D \geq 10,000 \\ \frac{L}{D} \geq 10 \end{array} \right]$$

$$(T_s > T_m) \Rightarrow n = 0.4$$

The average heat transfer coefficient,  $\bar{h}$ , can be determined from the average Nusselt number.

$$\bar{Nu} = \frac{\bar{h}L}{k_f} \quad (12)$$

Similar to Equation (4), the mean temperature,  $T_m$ , is used as a reference temperature for internal comparable to the free stream temperature for external flows. Newton's law of cooling can be expressed as in Equation (13).

$$q'' = h(T_s - T_m) \quad (13)$$

The total cooling jacket heat transfer rate can be determined by using the specific heat of the cooling water and the change in temperature from the inlet to outlet of the cooling jacket. Equation (14) is an appropriate general equation that applies regardless of the nature of the surface thermal or tube flow conditions [7].

$$q_{conv} = \dot{m} c_p (T_{m,out} - T_{m,in}) \quad (14)$$

The mean temperature in  $T_{m,in}$ , and the mean temperature out  $T_{m,out}$ , are measured by a thermocouple. The mass flow is physically measured; therefore, the heat flux is determined by dividing the heat transfer rate by the inner surface area of the cooling jacket. After the Nusselt number is determined, the average heat transfer coefficient is found by using Equation (12). The surface temperature of the cooling jacket wall is then evaluated using the heat flux from Equation (14). By knowing the surface temperature of the cooling jacket wall, the surface temperature on the inside wall of the combustor is resolved by conduction in Equation (3).

### **3. Convection Along the Combustor Inner Wall**

Convection along the inner wall of the combustion chamber is very difficult to evaluate based on the continuously changing flow conditions due to detonation and refresh periods. Even if the combustor always had a steady flow, in order to consider fully developed turbulent flow, the length of the combustor would have to be ten times the hydraulic diameter. Since the diameter of the combustion chamber is 7.62 cm, a  $L/D$  ratio greater than ten would require the combustor length to be greater than 30" in length. This condition is not met, therefore, the Nusselt number calculation in Equation 11 cannot be used to aid in calculating the heat transfer coefficient. The thermal boundary layer thickness is zero at the tube entrance and the convection coefficient would be extremely large at this location. As the thermal boundary develops, the convection coefficient decays rapidly.

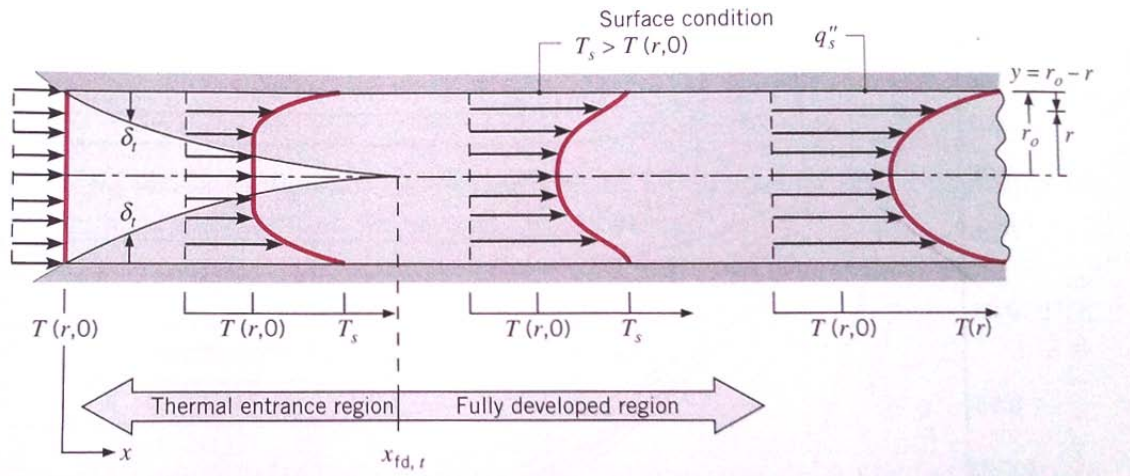


Figure 8. Thermal Boundary Layer Development in a Heated Circular Tube (From [7])

Since the heat flux across the tube wall is known, an alternate approach using Equation 13 can be used to determine the effective heat transfer coefficient of the inside combustor wall. One expectation is that since detonation does not occur until after the installed ramps, the observed heat transfer rate will vary axially depending upon the location inside the combustion chamber.

### III. DESIGN AND EXPERIMENTAL SETUP

#### A. PULSE DETONATION ENGINE

The experimental testing occurred at the Rocket Propulsion Laboratory (RPL), an off-campus testing facility that is part of the Naval Postgraduate School in Monterey, California. The PDC and a majority of the equipment used for testing were located in Test Cell #2. Additional equipment was located in Test Cell #3 and in the Control Room. The test equipment included the combustor section, cooling jackets, ethylene/air delivery systems, cooling water system, data acquisition system, and PDC controller. Most of the equipment was used in previous experimentations; however additional thermocouples and pressure transducers were added to accurately monitor various water jacket conditions.

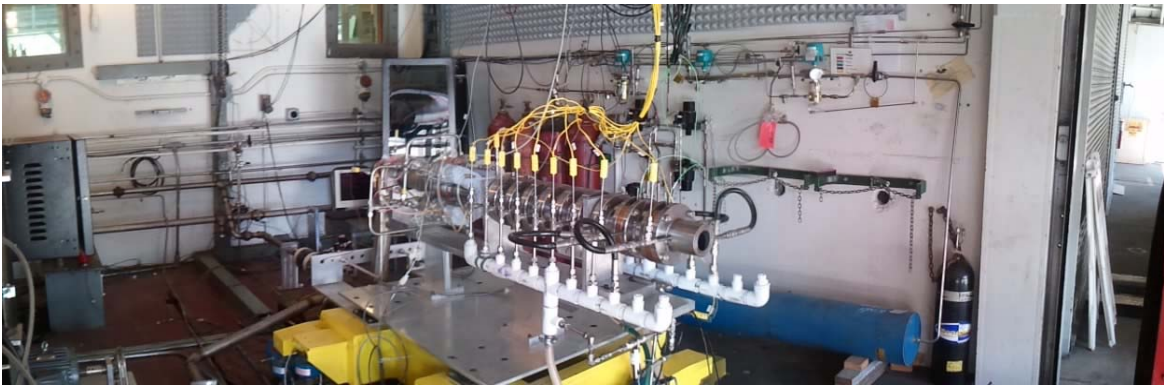


Figure 9. Naval Postgraduate School Rocket Propulsion Laboratory Test Cell #2

The valve-less single tube PDC design at NPS has continuously evolved through research by graduate students for the past six years. The PDC consists of a fuel and air injection system, an ignition system, and a combustion chamber that is coupled with a cooling water system. The fuel injector and ignition system is connected to the PDC controller and all of the diagnostics are recorded by a data acquisition system to determine performance.

## **B. FUEL AND AIR DELIVERY**

### **1. Air**

The supply air was delivered to the PDC by a 5.08 cm diameter supply line after being heated by a vitiator. This allowed for simulation of various combustor inlet conditions. The vitiator operated by injecting hydrogen into the main air supply flow, which was then ignited with a hydrogen/air torch. Hot air from the vitiator heated the PDE downstream piping and combustor to the desired conditions. This was accomplished by running the vitiator for approximately 15 seconds. Air temperature remained steady for several seconds after the vitiator was turned off, but cooler incoming air would be experienced by the PDE for longer duration runs.

The heated air was split and delivered to the combustor through four 3.81 cm fueling arms where fuel was added to the air. In each of the inlet arms, chokes were installed in order to separate the vitiator from downstream pressure oscillations. By splitting the air and fuel into four separate arms, proper fuel/air mixing occurred while providing a more even injection of the fuel/air mixture into the combustor.

### **2. Ethylene**

Controlled delivery of the ethylene fuel in a time-varying manner is necessary in order to supply proper stoichiometry of the fuel/air mixture provided to the combustor. Varying the mass flow rate of the injected fuel was accomplished by varying the supply pressure with Tescom regulators. The varied fuel injection pressure adjusts the mass flow rate of the fuel thereby dictating the equivalence ratio ( $\phi$ ) of the mixture for each engine cycle. In Equation 15, the equivalence ratio is determined by dividing the mass ratio fuel to air used in testing by the mass ratio of fuel to air for the stoichiometric condition.

$$\phi = \left[ \frac{\left( \frac{F}{A} \right)}{\left( \frac{F}{A} \right)_{ST}} \right] \quad (15)$$

The highest thrust values occur when the equivalence ratio of the fuel/air mixture is near unity. If the mixture is rich or an equivalence ratio greater than unity, fuel will left unburned since there is more fuel that can be combusted for the given amount of oxidizer. Lower specific impulse is the result of the wasted fuel while still producing similar thrust levels. In opposition, a lean mixture that yields an equivalence ratio less than unity result in lower thrust values, but can generate higher fuel-based specific impulses.

$$I_{sp} = \frac{I_t}{(m_p g_o)} = \frac{F}{(\dot{m} g_o)} \quad (16)$$

$$I_{SP_f} = \frac{F}{(\dot{m}_f g_o)} \quad (17)$$



Figure 10. Test Cell 2 Fuel and Gas Tanks

Ethylene is delivered to the PDC from an accumulator installed prior to the research performed by Nichols [8]. The installed accumulator allows for constant pressure delivery of ethylene and longer duration runs of the PDC in which both are required to generate steady-state heat transfer condition. The blue accumulator in Figure 10 has a piston that is pressured inside a cylindrical pressure vessel. Ethylene fills the accumulator on one side of the piston, and nitrogen gas pressurizes the ethylene by

supplying the required pressure on the other side. Pressure of the nitrogen gas was controlled by Tescom regulators. The pressurized ethylene is supplied to the PDC at the required pressure.

Four independent injectors located in four fuel arms were used to supply ethylene to the PDE. A common feed manifold with four electronically-controlled high frequency Valvetech (PN#15060-2) solenoid valve injectors were mounted to the fuel arms downstream of the flow chokes. Supplied air was mixed with the gaseous fuel mixture prior to entering the combustion chamber. One of the two new fast response Vavletech (PN#12177-2) solenoid valve injectors used by Nichols [8] was defective and returned to the factory for service.

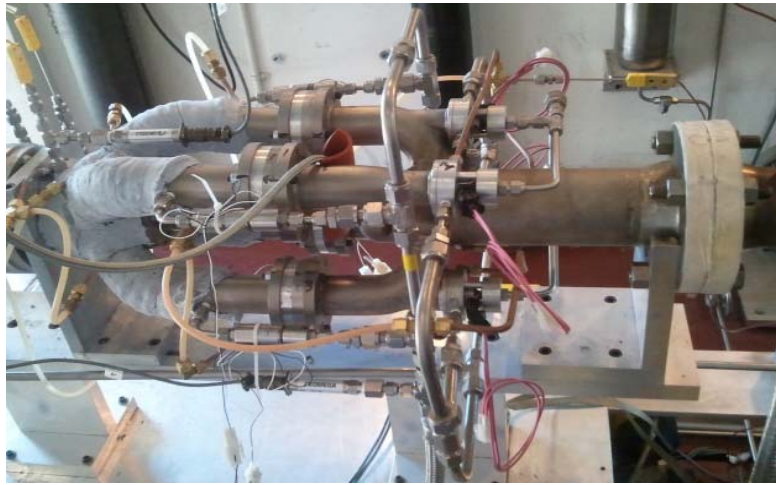


Figure 11. PDE Fuel Arms and Injectors

### 3. Ignition System

A small-scale Transient Plasma Ignition (TPI) system was used to control the ignition of the PDC. A TPI box generates a high voltage signal to an electrode assembly. The electrode assembly is inserted into the combustion chamber through a machined orifice. The BNC 500 Pulse generator pulsates at a preset frequency to the BNC 575 in order to produce two output waveforms for each pulse. These waveforms provide a

signal to produce a rapid charge input to the High Volt Pulse Generator. The electrode then develops a corona discharge to the electrode shroud. The TPI cycle is displayed in Figure 12.

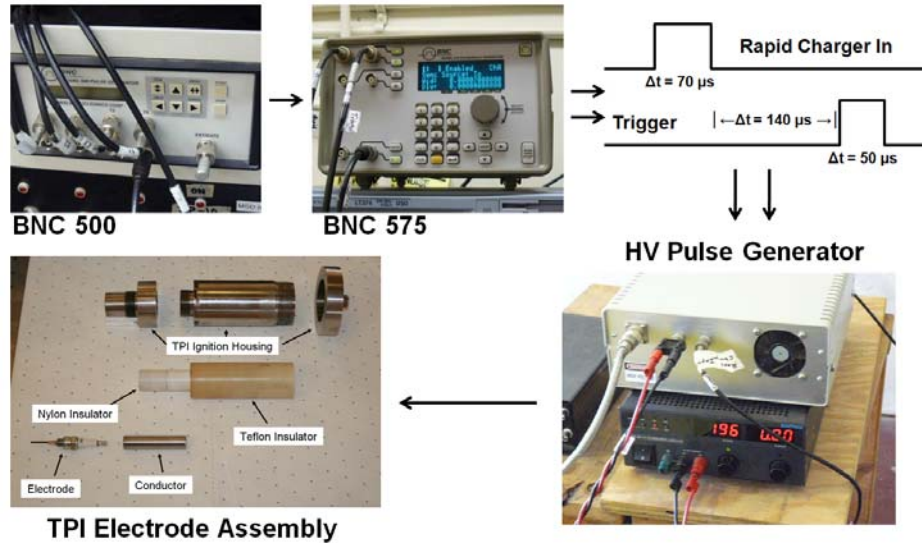


Figure 12. Flow Path for Transient Plasma Ignition (From [6])

The electrode shroud pictured on the left in Figure 13 was used on multiple runs of the PDC. During runs of five seconds or longer, flame holding was obviously present in the PDC exhaust. The long shroud was suspect of causing auto ignition of the fuel/air mixture due to the high shroud temperatures during extended runs. The shroud was cut to various shorter lengths to minimize the potential for flame holding to occur and did improve the engine operation.



Figure 13. TPI Electrode Shroud

## C. COMBUSTOR ASSEMBLY

### 1. Combustor

The combustor assembly consisted of a 7.62 cm diameter combustion tube with a convergent divergent nozzle on the end. The eight combustion tube sections and the nozzle were assembled together to form the complete combustor assembly. Each section was made of 4340 steel and has a cooling jacket that is supplied by the cooling water system.

The primary combustion tube consisted of eight 7.62 cm sections for an overall length of 0.6096 m. The combustor section had a 7.62 cm inside diameter and it was constructed from 4340 annealed steel. Each section was a two piece assembly designed by Thomas Lipoma, a NPS RPL summer intern student. The inner tube was pressed into an outer casing with flanges on both ends to allow each section to be bolted together. An O-ring was inserted into the groove on the aft flange face to insure proper sealing between each section. The combustor had an inner wall thickness of 0.3175 cm to separate combustion gases from the cooling water.

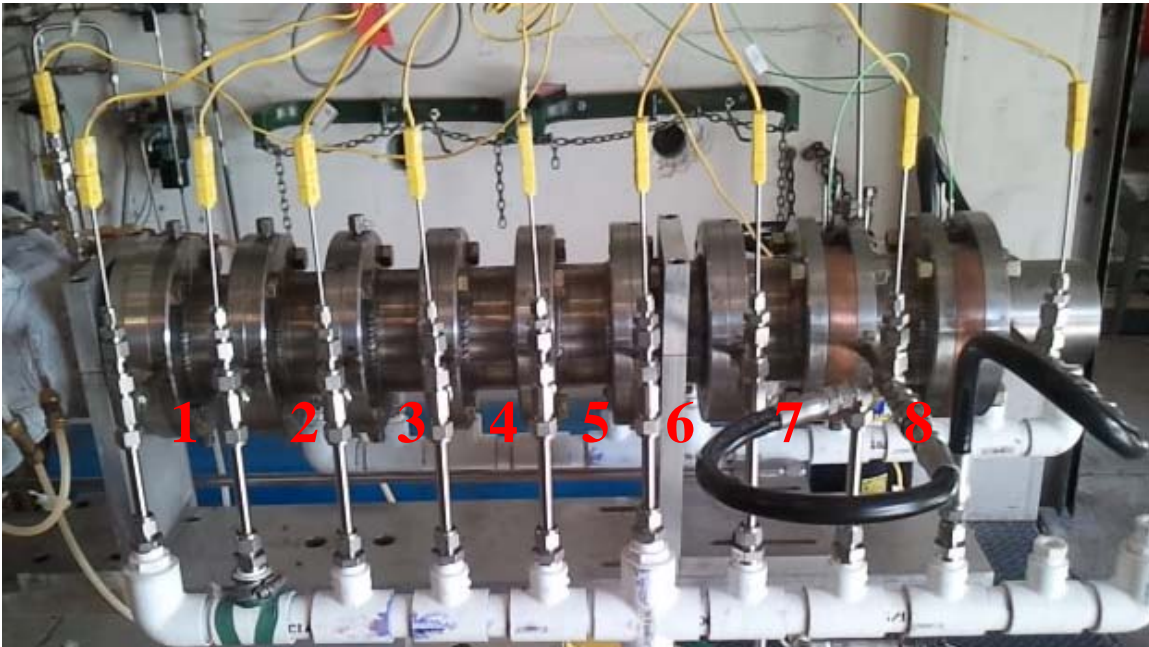


Figure 14. PDE Combustor

Each section had a hole drilled in the aft flange that penetrated through the combustor wall. The holes were 180 degrees apart at the top and bottom of the combustor tube. Each hole allowed for the installation of an obstacle onto the combustor inner wall. The obstacles are discretely placed along the combustor wall to achieve DDT. The preferred obstacle shape to achieve a balance between detonation initiation performance and pressure loss was determined by research conducted by Dvorak [6]. The obstacle designed was a swept ramp in a configuration known as 2R.180.4S [6] as seen in Figure 15.



Figure 15. Dvorak Swept-Tall Ramp (From [6])

This research used four sets of ramps placed in combustor sections four through seven. Each ramp was bolted in place with a thin layer of Room Temperature Vulcanizing (RTV) silicone rubber between the ramp and the combustor wall. In the sections that did not utilize the use of an obstacle, the drilled holes were plugged with a cap and lock wired into place.

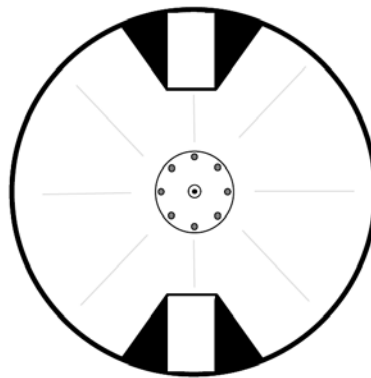


Figure 16. Swept Ramp Configuration Inside Combustor [From (8)]

## 2. Cooling Jackets

The channels in between the inner tube and the outer casing allowed for the passage of cooling water and can be seen in Figure 17. A cooled combustion chamber was required due to the extreme temperatures and pressures experienced during the operation of the PDE. By cooling the combustor, the wall could maintain its integrity during extended durations. Part of this research was to determine the amount of cooling required of the combustor wall to achieve sustained operation of the PDE.



Figure 17. PDE Cooling Jacket

Each water cooling channel was 0.635 cm wide by 0.635 cm high. In each 7.62 cm combustor section, the channel wrapped around the combustor eight times in order to achieve a channel length slightly greater than 0.762 m. Each of the eight sections was attached to a common supply manifold and a common discharge manifold. Mass flow rates were measured at various differential pressures through each combustor section to accurately determine the amount of heat transfer occurring through the combustor wall to the cooling water.

### 3. Cooled Nozzle

A two-piece nozzle assembly similar to the combustor section utilized inner channels to allow a passageway for cooling water. The convergent-divergent nozzle was design with a 15 degree half angle and was 9.21 cm in length. The nozzles was designed by NPS RPL intern student and used in the research conducted by Nichols [8]. A detailed drawing can be viewed in Appendix B.

### 4. Cooling Water System

The cooling water system provided cooling water through each combustor and the nozzle section to limit the combustor bulk wall temperature. Cooling water was delivered to the combustor from a 115 gallon cooling water tank via a MTH brand regenerative turbine pump, Model 284K BF with a capacity of 60 GPM. The supply line pressure maintained 69000 Pa with a 20700 Pa differential pressure across the supply and discharge manifolds. The position of the recirculation line ball valve determined the system operating pressure as well as the differential pressure across the manifolds. A cooling water system diagram is included in Appendix B.



Figure 18. Cooling Water Tank (Left) and Regenerative Turbine Water Pump (Right)  
(From [8])

The cooling water system delivered the required mass flow rate in order to achieve proper cooling of the exterior combustor wall by means of forced convection. A common thermocouple and pressure transducer were installed on the supply manifold. On the discharge manifold, individual thermocouples were installed to monitor the outlet temperature of each cooled combustor section and the cooled nozzle. A differential pressure cell was connected between both manifolds to determine the average pressure drop through the cooling jackets.

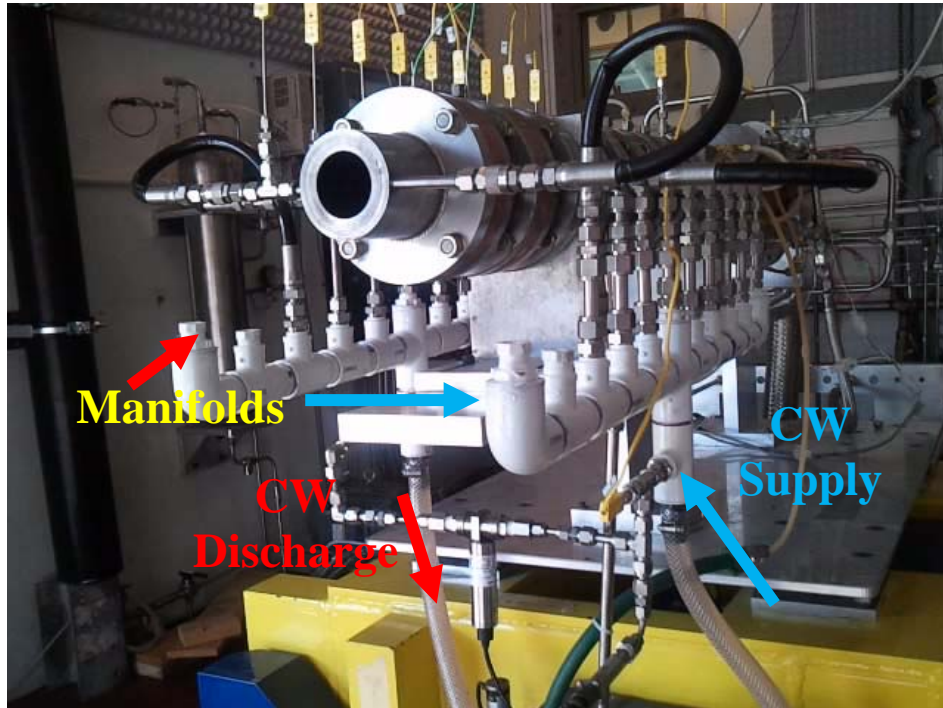


Figure 19. PDE Cooling Water Supply and Discharge Manifolds

A separate system provided cooling to each of the four fuel arms. Water was supplied by RPL potable water and the piping wrapped around the fuel arms. The piping was then enclosed by thermal paste. The thermal paste can be seen on the fuel arms in Figure 11.

## D. INSTRUMENTATION

### 1. Thermocouples

Type K thermocouples from Omega Engineering, Inc. were used to measure temperatures at various locations. Each K type thermocouple is rated up to 1335 degrees C with a response time of 0.55 seconds. Each thermocouple was wired to the data acquisition system into National Instrument's TC-2095 rack-mounted analog breakout accessory. Table 1 lists all the thermocouple temperatures recorded by the data acquisition system.

Table 1. Thermocouple Connections

<b>Thermocouple #</b>	<b>Device</b>	<b>National Instrument TC-2095</b>
1	Vitator	CH 00
2	Engine Inlet	CH 01
3	Cooling Water Inlet	CH 02
4	Cooling Water Discharge 1	CH 03
5	Cooling Water Discharge 2	CH 04
6	Cooling Water Discharge 3	CH 05
7	Cooling Water Discharge 4	CH 06
8	Cooling Water Discharge 5	CH 07
9	Cooling Water Discharge 6	CH 08
10	Cooling Water Discharge 7	CH 09
11	Cooling Water Discharge 8	CH 10
12	Cooling Water Nozzle Discharge	CH 11

## 2. Pressure Transducers

Several pressure transducers and one differential pressure cell were installed to monitor and record operating of the PDE and cooling water systems. The pressure transducers used were fabricated by Omega Engineering, Inc Model PX613. Each transducer is ideal for gas or liquid with an accuracy of 0.4%. Also, one Honeywell differential pressure cell, Model FDW, was connected to measure the differential pressure across the cooling water manifolds. All pressure cells were connected to National Instruments' BNC 2090A rack-mounted analog breakout accessory. Table 2 lists the systems measured and recorded pressures by the data acquisition system.

Table 2. Pressure Transducer Connections

<b>Pressure Transducer</b>	<b>Range (GPa)</b>	<b>Device</b>	<b>National Instrument BNC-2090A</b>
1	0-13.8	Main Air Supply	AI7
2	0-13.8	Ethylene Supply	AI8
3	0-13.8	Hydrogen Supply	AI9
4	0-1.38	Cooling Water	AI10
5	69000 Pa differential	Cooling Water D/P	AI11
6	0-13.8	Engine Inlet	AI12
7	0-1.38	Shop Air Supply	AI13

## 3. Kistler Pressure Sensors

Two Kistler 603B1 piezoelectric pressure transducers were inserted into the Kistler 228P cooling jackets. Each unit was installed into a copper spacer placed between to combustor sections. The copper section was designed by Nichols [8] to allow penetration of the Kistler probe close to the combustion chamber inner wall just aft of the last set of swept ramp obstacles installed. These probes are capable of high frequency pressure measurements under the extremely high operating temperatures of detonation.



Figure 20. Kistler Pressure Sensor and Kistler Cooling Jacket (From [8])

Mechanical stress due to a pressure wave passing by each of the Kistler probes electrically charges the piezoelectric crystals, which then provide a charge proportional to the force experienced by the crystal. The charge is measured in picocoulombs (pC) and was transmitted to a Kistler 5010 multi-charge amplifier to convert and amplify the signal to a proportional voltage. The scale of the amplifier was set to 100 MU/volt with a sensitivity of 0.380 pC/MU. By knowing the distance between the two probes, the elapsed time measured between the pressure spikes of each probe can determine the speed of the pressure wave. An indication that detonation occurred comes as a result of a wave speed in excess of 1,500 m/s.



Figure 21. Kistler Amplifiers

## E. DATA ACQUISITION

The data acquisition was recorded by two National Instrument Graphical User Interface (GUI) programs. The Kistler high speed pressure data was recorded by GUI pictured in Figure 22. At the moment the PDE was ignited, an operator would depress the “Start Data Recording” and three seconds of high speed data was logged. The graph presented in the LabView program displayed the results that allowed immediate analysis of the PDE operation. The saved data was later analyzed in further detail to ensure adequate detonations were occurring.

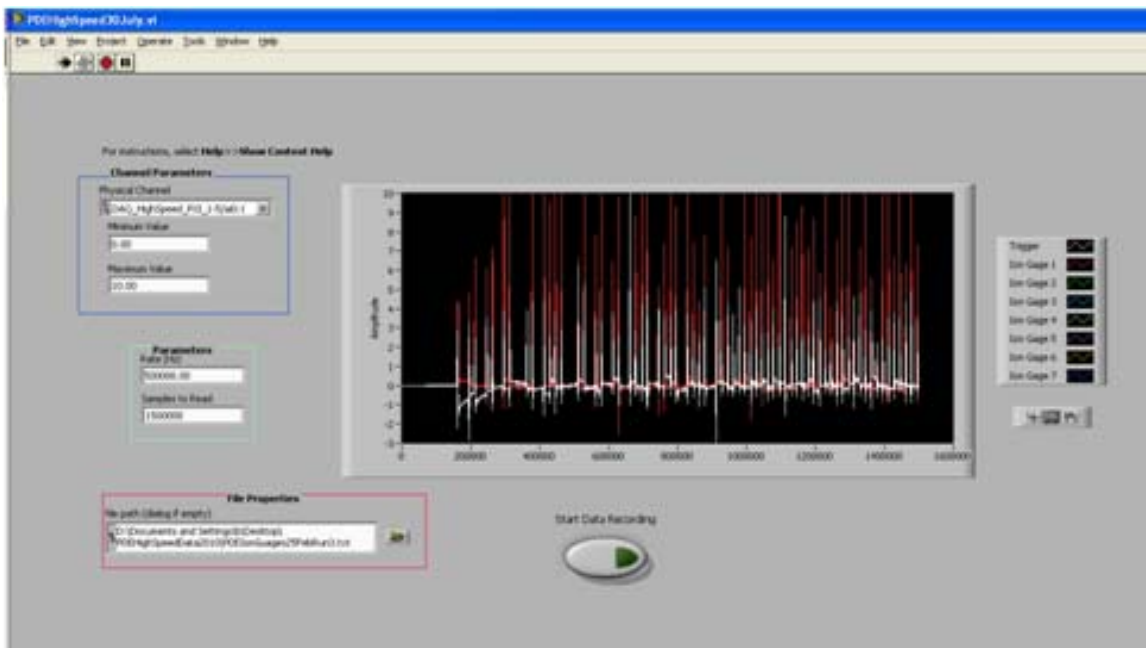


Figure 22. National Instruments LabView Data Acquisition System

The pressure and temperature data was recorded by the GUI pictured in Figure 23. The LabView program served as a sequence controller for the operation of the PDE and also as data acquisition. Temperature and pressure parameters were present in real time on the screen to aid the operator in the proper operation of the PDE, and also were recorded for aiding in the troubleshooting of the PDC operation if necessary. The logged pressure and temperature data was analyzed to determine corresponding heat transfer characteristics.

## F. PDE CONTROLLER AND OPERATING PROCEDURE

Two National Instruments LabView programs served as the controllers for the PDC. Each program was installed on separate computers and controlled by two operators in the RPL control room. One computer was connected to a National Instruments PXIe-1062Q controller and the National Instruments PXI-1000B controller was connected to a different computer. Together, these two programs set the operation conditions of the PDE and remotely controlled the gas supply valves located in the test cell although the main air supply and cooling water flow was controlled by two manual switches in the control room. For safety considerations, the ignition of the PDE occur manually by an operator and the operator was capable of stopping the ignition sequence. For further safety, two emergency shutoff buttons are located in the control room. By depressing the shutoff buttons, fuel injection and ignition trigger signals were disrupted and placed the PDC in a safe condition by disabling the test cell.

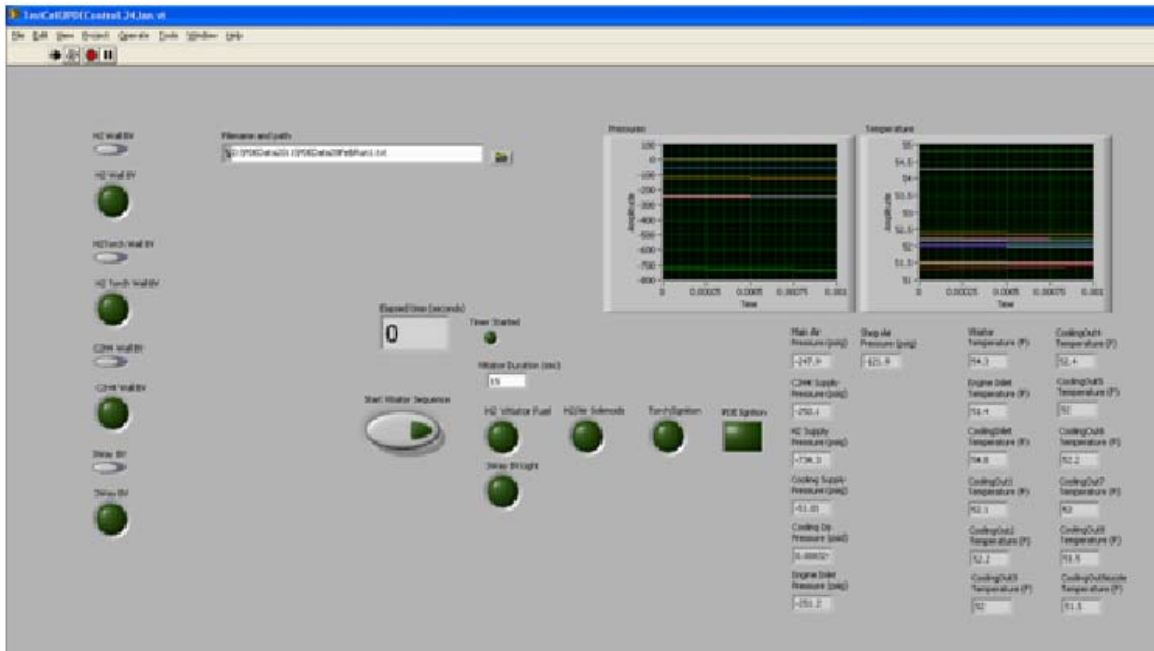


Figure 23. National Instruments LabView Test Cell #2 PDE Controller 1

The GUI pictured in Figure 24 sets all the parameters of the PDC including frequency, number of cycles, fill times and ignition delay times. Once engine parameters were set, the main air supply was initiated followed by depressing the “Start Sequence” button on the GUI in Figure 23. This controller operated the position of the gas valves, started the vitiator sequence, and provided the countdown to manually ignite the PDE. A standard operating procedure was put into place to ensure proper valve lineup for PDE startup, proper sequence for ignition, and to provide a safe condition directly after a run was complete as well as for a complete shutdown of the PDE.

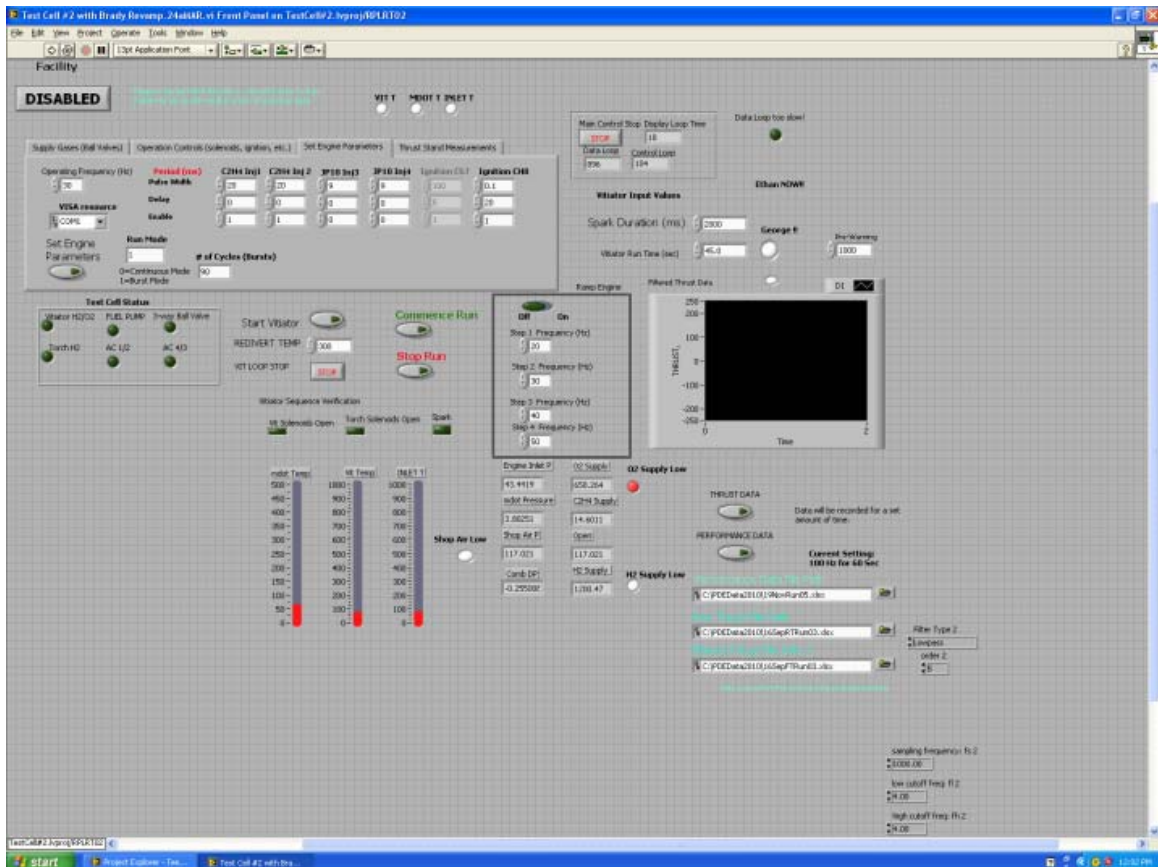


Figure 24. LabView Interface Controller (From [8])

## G. COOLING WATER MASS FLOWRATE

Testing was performed on the cooling water system to calculate the mass flow rates of the cooling jacket sections at various differential pressures. For each cooling jacket section, the cooling water outlet was disconnected from the cooling water

discharge manifold. While maintaining a constant differential pressure across the cooling jacket, cooling water was collected into a 2000-milliliter beaker for a prescribed amount of time. The mass of the water in the beaker was measured with a digital scale. This process was repeated three times, and the mass was averaged to minimize errors due to the natural inconsistencies in the time recording evolution. Each cooling jacket was tested in this manner at a set differential pressure. The entire process would then be repeated at various differential pressures by adjusting the position of the recirculation valve in the cooling water system.

Using the recorded water mass for each calibration point, water temperature, and time, mass flow rates for each cooling jacket were calculated for various differential pressures. It was observed that the mass flow rates for each individual cooling jacket were varied by a common factor between the two differential pressures.

Since the mass flow rate varied by the same amount for each cooling jacket, only additional measurements were taken using Cooling Water Jacket #6 mass flow rate at different pressures. After plotting the mass flow rates against differential pressure, it was noted that each cooling water jacket had approximately the same slope for a given differential pressure change.

Table 3. Various Cooling Water Mass Flow Rates

Mass Flow Rate		Differential Pressure (kPa)			
		6.89	13.8	20.7	27.6
<b>CW1</b>	(g/s)	61.61	72.32	83.02	93.73
<b>CW2</b>	(g/s)	61.57	72.28	82.98	93.69
<b>CW3</b>	(g/s)	61.28	71.99	82.69	93.40
<b>CW4</b>	(g/s)	62.49	73.20	83.90	94.61
<b>CW5</b>	(g/s)	61.28	71.99	82.70	93.40
<b>CW6</b>	(g/s)	57.67	68.37	79.08	89.79
<b>CW7</b>	(g/s)	58.06	68.77	79.48	90.18
<b>CW8</b>	(g/s)	57.43	68.13	78.84	89.55
<b>CWnozzle</b>	(g/s)	48.57	59.28	69.98	80.69

## H. PRESSURE TRANSDUCER CALIBRATION

Calibration of the pressure transducers was necessary to ensure proper accuracy of the recorded data from each pressure transducer. Each transducer was connected to a Heise gauge and nitrogen gas bottle. A regulator was used to pressurize each transducer to several predetermined set points. Once pressure was stabilized on the Heise gauge, the transducer output voltage was recorded. The recorded data was used to develop an equation of a line and the data was entered into the LabView program.

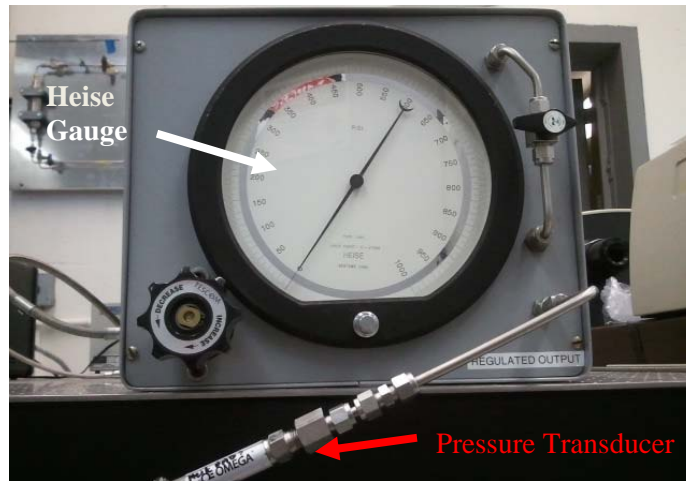


Figure 25. Calibration of Pressure Transducers

Table 4. Pressure Transducer Calibrations

<b>Pressure Measurements</b>	<b>Calibration Data</b>
Cooling Water	$P = 50.18V - 51.17$
Ethylene	$P = 250.2V - 250.0$
Main Air	$P = 250.1V - 250.0$
Engine Inlet	$P = 249.7V - 251.6$

## **IV. EXPERIMENTAL RESULTS**

The PDC was operated with ethylene/air mixtures to gather heat transfer characteristics while operating at different frequencies and fuel fill times. By keeping the fill duration constant and varying frequency, the amount of time that purging occurs relative to the filling of fuel and air was altered and directly affected the amount of cooling provided by the purge and refresh portion of the cycle. By increasing frequency, the number of cycles per second increased the aggregate amount of heat generated by the PDC. Lastly, by changing the fuel filling times, the amount of fuel available for detonation was also varied thus affecting the amount of heat produced for each fuel cycle. By testing at various frequencies and fill times, the variation of the inner combustor wall was observed as well as the effective heat transfer coefficient.

Measuring the temperature differential across each cooling jacket provided heat transfer results at multiple locations along the combustor axis. Using the conduction and convection equations from Section III, the cooling water temperatures can approximate the combustor wall temperatures along its entire length.

### **A. TESTING AT 20 HZ**

The PDC was operated at a frequency of 20 Hz with a stoichiometric ethylene/air mixture fill time of 20 milliseconds. It was determined the cooling water outlet temperatures reached a steady state condition after about 18 seconds of operation.

In Figure 26, the cooling water temperature differentials and the cooling water mass flow rates through each individual cooling jacket was used to determine the average heat transfer rate in Watts. The maximum observed heat transfer occurred at Cooling Water Jackets 7 and 8. These two cooling water jackets are positioned just aft of the last swept ramp obstacle in the combustor tube. The position of the last ramp has been observed during previous testing to be the location where detonation initiation occurs and therefore produces high temperature and pressures from the detonation event. The maximum heat transfer rate is observed at approximately 12 kilowatts while the minimum is around 9 kilowatts.

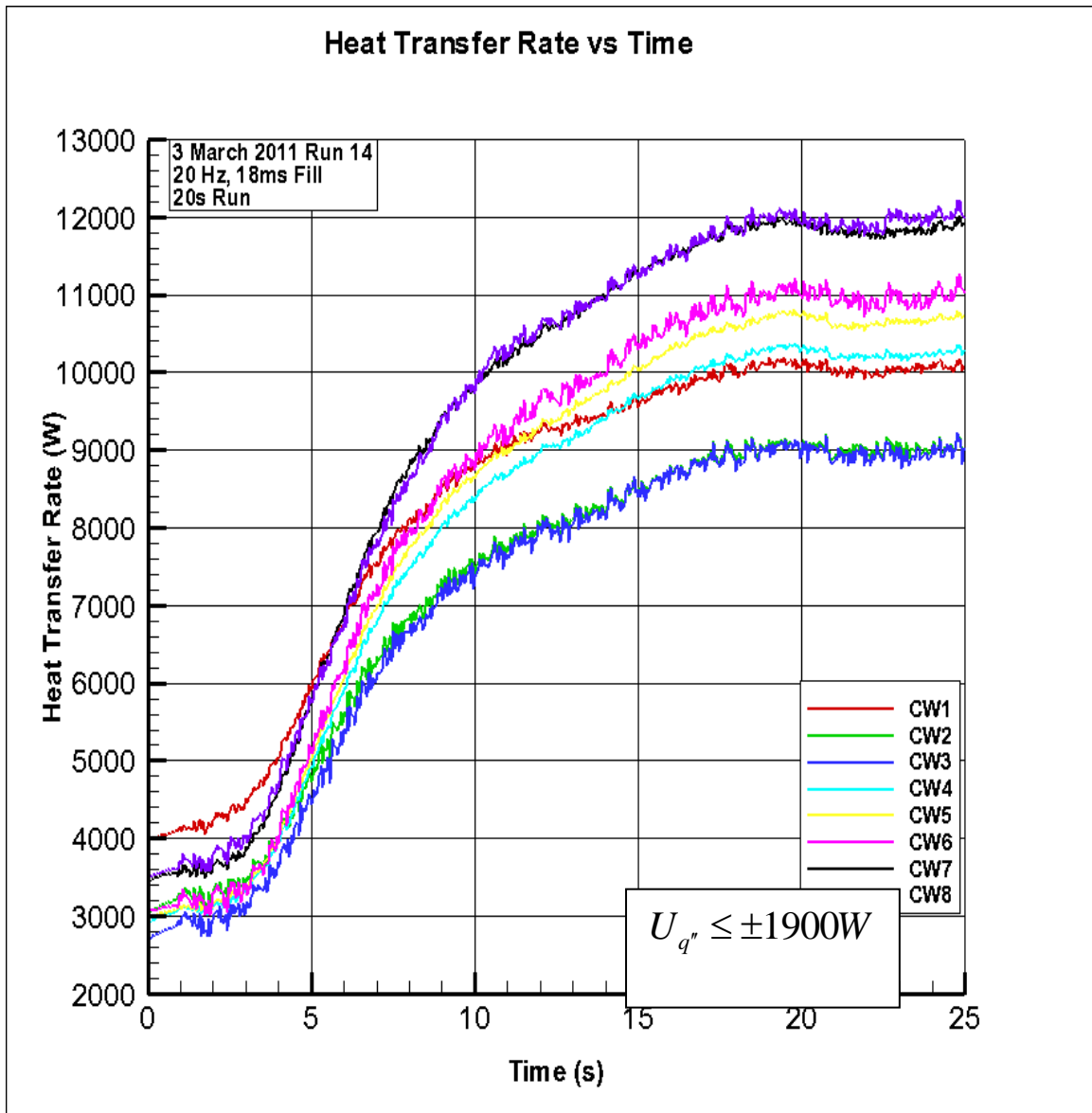


Figure 26. Heat Transfer Rates for 20 Hz Tests

Using the heat transfer rates and the mean cooling water temperature for each cooling water jacket, the liquid-side wall temperature of the cooling water jacket was calculated. The calculated cooling water jacket wall temperature was then used with the conduction equations to calculate the inside wall temperature of the combustor,  $T_{g,wall}$ . In Figure 27, the maximum  $T_{g,wall}$  occurs at Cooling Water Jackets 7 and 8, which corresponds to the maximum heat transfer rates. The maximum combustor wall

temperature was determined to be slightly less than 130° C. The cooling water differential pressure was set to approximately 20,700 Pa during the 20 Hz tests. This flow rate is achieved by setting the recirculation line to full open position allowing the minimum flow rate without adjusting the ball valve leading to Test Cell #2. A schematic of the Cooling Water System is located in Appendix B. The amount of cooling water mass flow provides more than adequate cooling of the combustor inner wall.

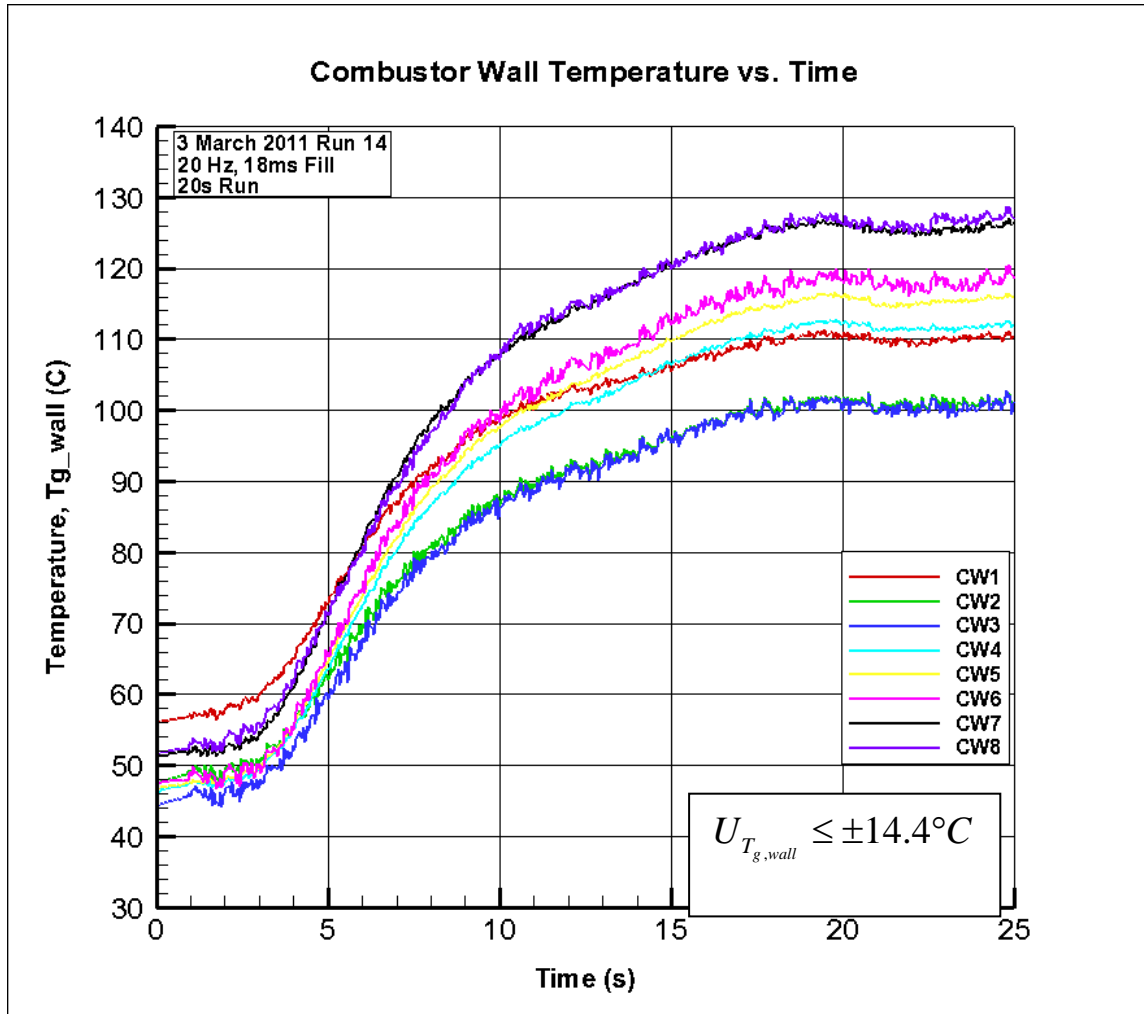


Figure 27. Combustor Wall Temperatures for 20 Hz Tests

Figure 28 displays the variations in combustor wall temperatures along the length of the combustor for time steps of 0, 5, 10, 15 and 20 seconds. The shape of the temperature profile remains nearly constant from the initial start to steady state

conditions. An increasing temperature is noticed from near the front of the combustor towards the end as DDT occurs with a maximum just prior to reaching the nozzle inlet.

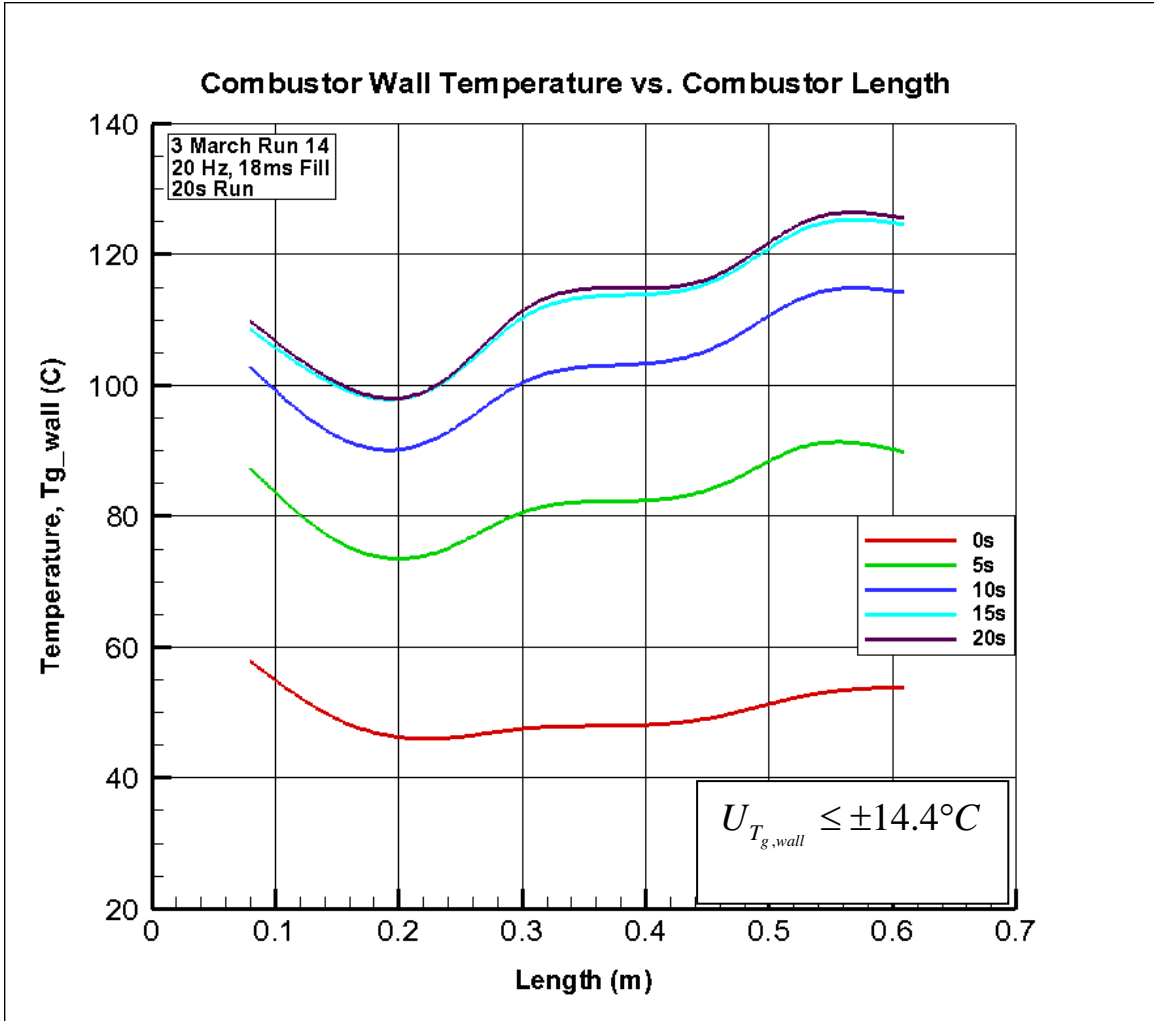


Figure 28. Combustor Temperature Profiles for 20 Hz Tests

## B. TESTING AT 30 HZ

Testing at 30 Hz with the same fill fraction produces 50% more detonations per second as compared to the 20 Hz testing. With many more detonations occurring, a noticeable increase in heat transfer rates and combustor wall temperature,  $T_{g,wall}$ , is observed. It is assumed that the increase in the number detonations per second caused some internal components in the combustor to reach temperatures above the auto ignition

point for ethylene gas/air mixture. Once the auto ignition temperatures were present, flame holding was observed in the PDC. The components assumed to be the source for auto ignition were either the ramp obstacles down the combustion chamber, the shroud that surrounds the Transient Plasma Igniter or a thermocouple directly in the flow field near the TPI unit.

The four sets of swept ramp obstacles were located at Cooling Water Jacket sections 3–6. The ramps are held in place by a retaining bolt placed through the flange of the cooling jacket. It was assumed that a small uniform layer of silicone existed between the ramp and the combustor wall due to the assembly technique, therefore minimizing the amount of heat transfer possible from the ramps to the cooling jacket. The thermocouple was also removed from the flow field to eliminate its potential as the source of the auto ignition. The shroud located at the front of the combustor is located along the centerline of the ignition region. The length of the shroud was cut to shorter lengths to attempt to provide improved cooling and minimize the chance of auto ignition. As the length of the shroud was shortened, the length of time prior to auto ignition occurring increased from about 5 seconds to 10 seconds. The source of auto ignition could not be isolated to either the TPI shroud or the swept ramp obstacles so tests at 30 Hz were limited to approximately 10 seconds.

Initial 30 Hz testing occurred with a fuel/air fill time of 18 milliseconds, which corresponds to fully filling the combustion chamber. In Figure 29, the maximum heat transfer rates occurred at Cooling Water Jackets 7 and 8, which is consistent with the 20 Hz testing. The maximum observed heat transfer rates reached approximately 15 kilowatts. Unfortunately, the heat transfer rates were not able to reach steady state conditions prior to the occurrence of auto ignition. The rates after 10 seconds of operation are greater than the steady state conditions reached at 20 Hz testing. The rate of change of the heat transfer rates at 10 seconds appears to be decreasing, which means it is attempting to start to level off to steady state conditions. It is assumed that steady state conditions would be reached in less than 20 seconds.

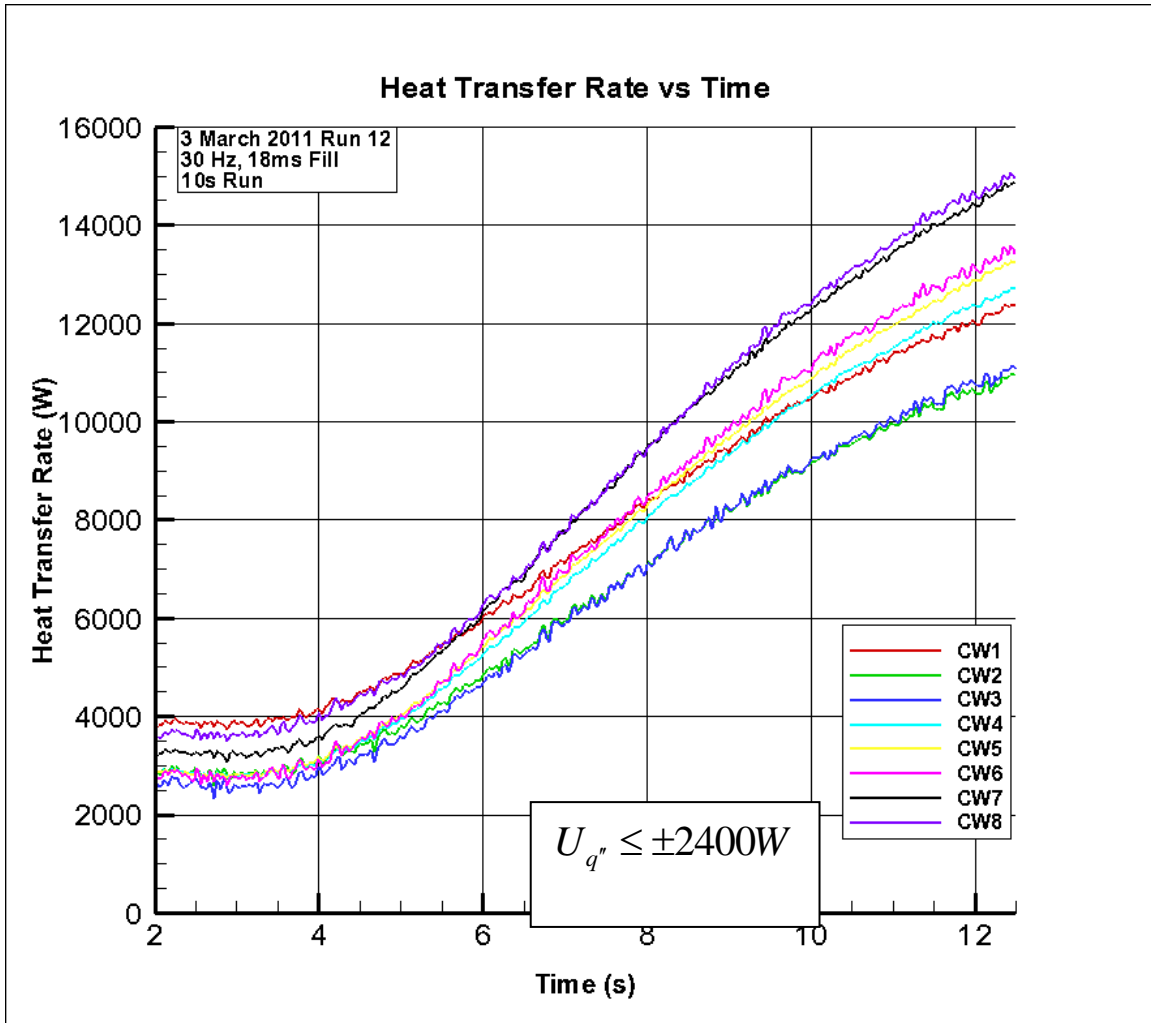


Figure 29. Heat Transfer Rates for 30 Hz Testing

In Figure 30, the heat transfer rate profiles along the length of combustion chamber for 30 Hz tests have the same shape as seen in the 20 Hz tests. The profiles shown are in two second intervals from 0–10 seconds with steadily increasing heat transfer rates along each time step. The front end of the combustor is producing about 11 kilowatts while the aft end where the DDT event occurs, experiences rates as high as 15 kilowatts prior to reaching a flame holding condition.

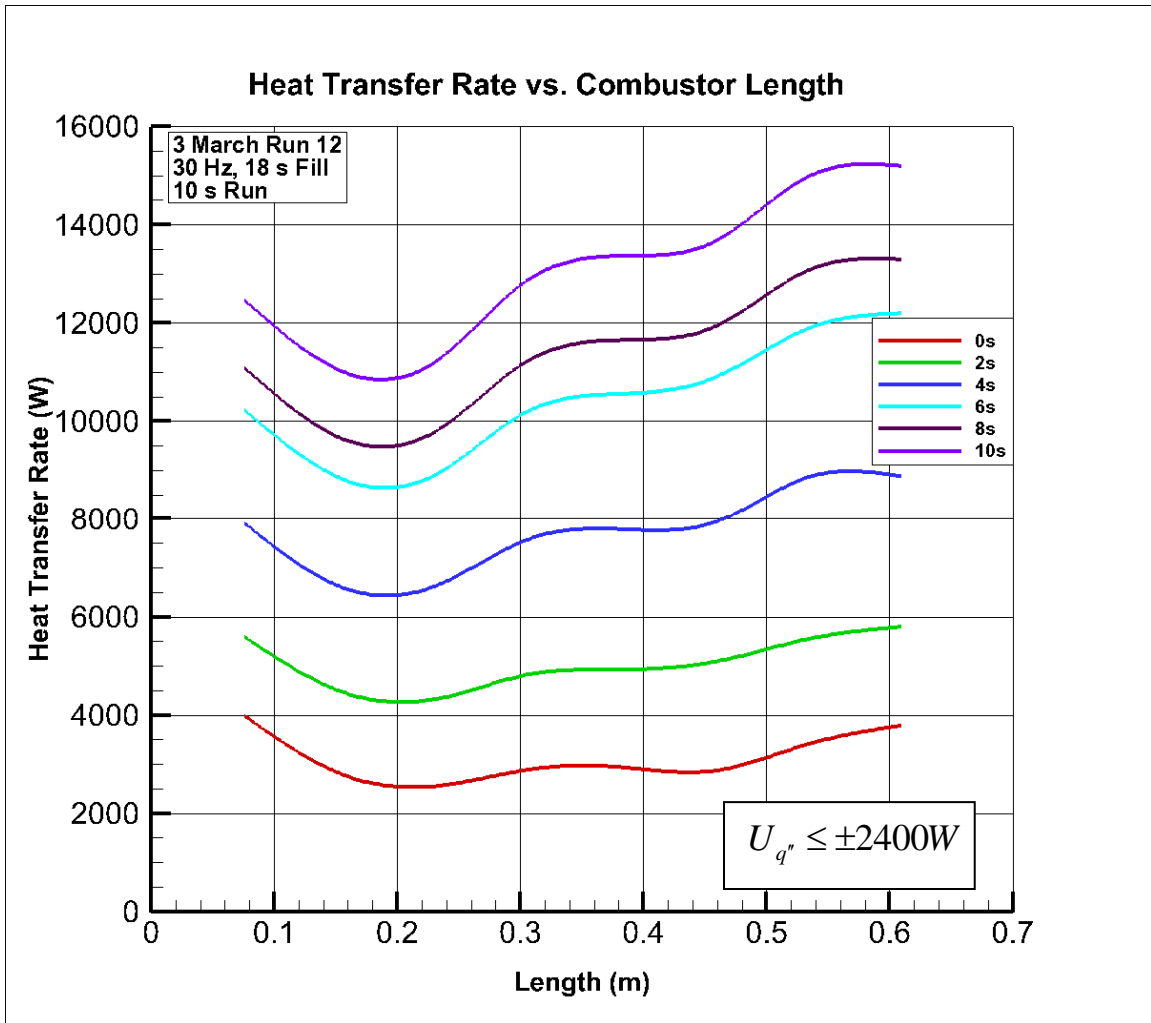


Figure 30. Heat Transfer Rate Profiles for 30 Hz Tests

The fuel fill times were varied from 14–18 milliseconds for 30 Hz operation to observe the changes in heat transfer. At 18 ms, fuel completely fills the combustion chamber and results in the greatest heat transfer rates and maximum combustor inner wall temperatures. Figure 31 displays a comparison of fill times of 14, 16, and 18 ms at Cooling Water Jacket 7. All three fill times produce combustor wall temperatures higher than the 20 Hz tests and it is obvious that the temperatures are still increasing and have not reach steady state in all three conditions. Even though steady state conditions were not achieved, it appears as if the inner combustor wall temperature would remain less than 180 degrees C. The outcome confirms that a partial fill of fuel in the combustion chamber results in a lower amount of heat transfer at the aft end of the combustor.

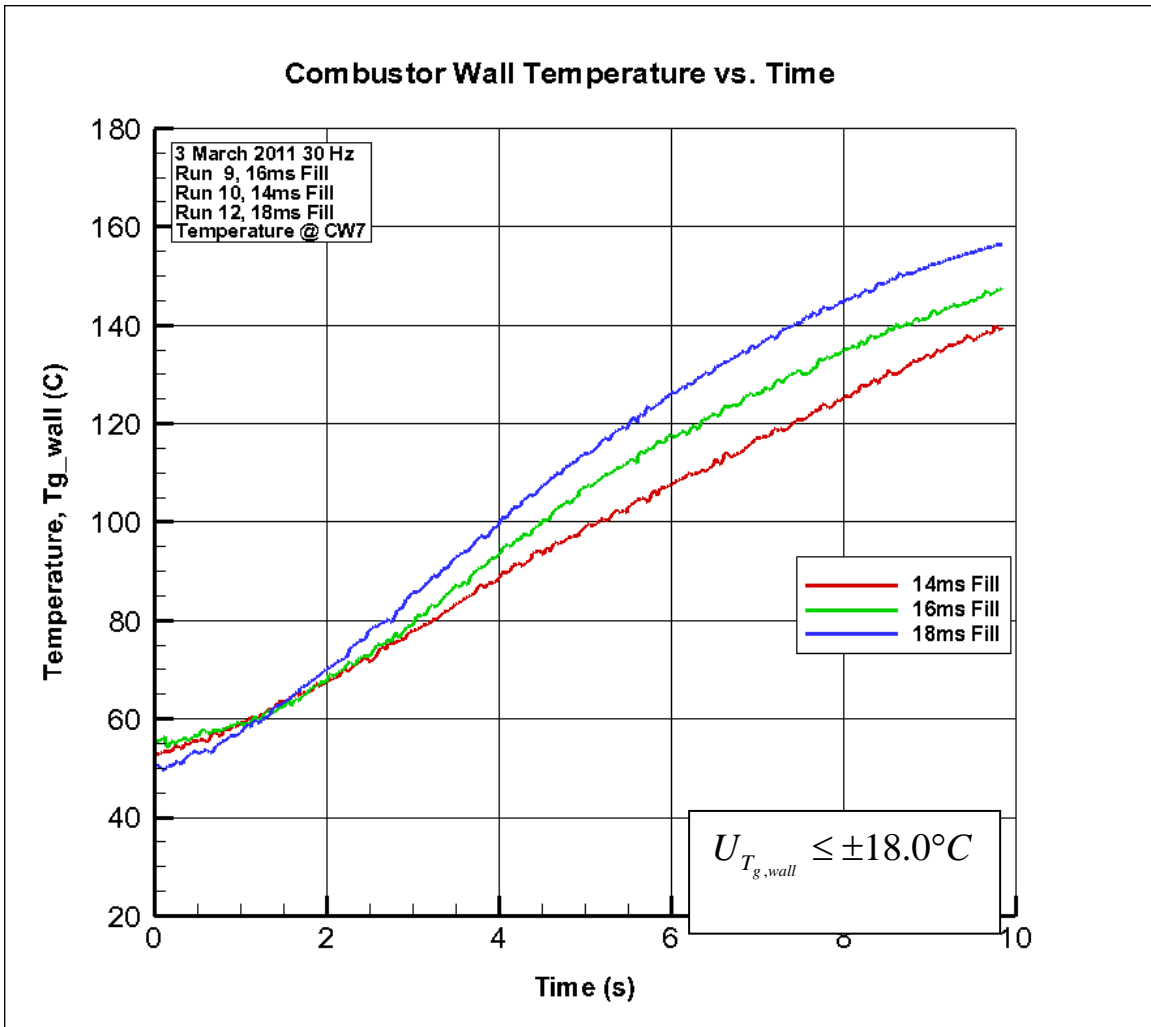


Figure 31. Combustor Wall Temperatures at CW7 for Fuel Fill Times of 14–18 ms

### C. COMPARISONS OF 20HZ AND 30 HZ TESTING

The results from 20 Hz and 30 Hz testing were compared since steady state conditions are reached during 20 Hz testing and not for 30 Hz. Comparisons were made with a fuel fill time of 18 ms, which corresponds to a full fill of the combustion chamber.

In Figure 33, the temperatures of 20 Hz and 30 Hz testing at Cooling Water Jacket 7 are compared. The 20 Hz testing occurred for 20 seconds while the 30 Hz testing was stopped after 10 seconds of operation. The 30 Hz temperature at 10 seconds reaches approximately 150 °C, which is about 30% greater than the 20 Hz temperature after 10

seconds of operation. It appears as if the 30 Hz testing were to reach steady state conditions then the inner combustor wall temperature would not exceed 200° C. At these temperatures, the combustor wall would be cool enough for extended operation.

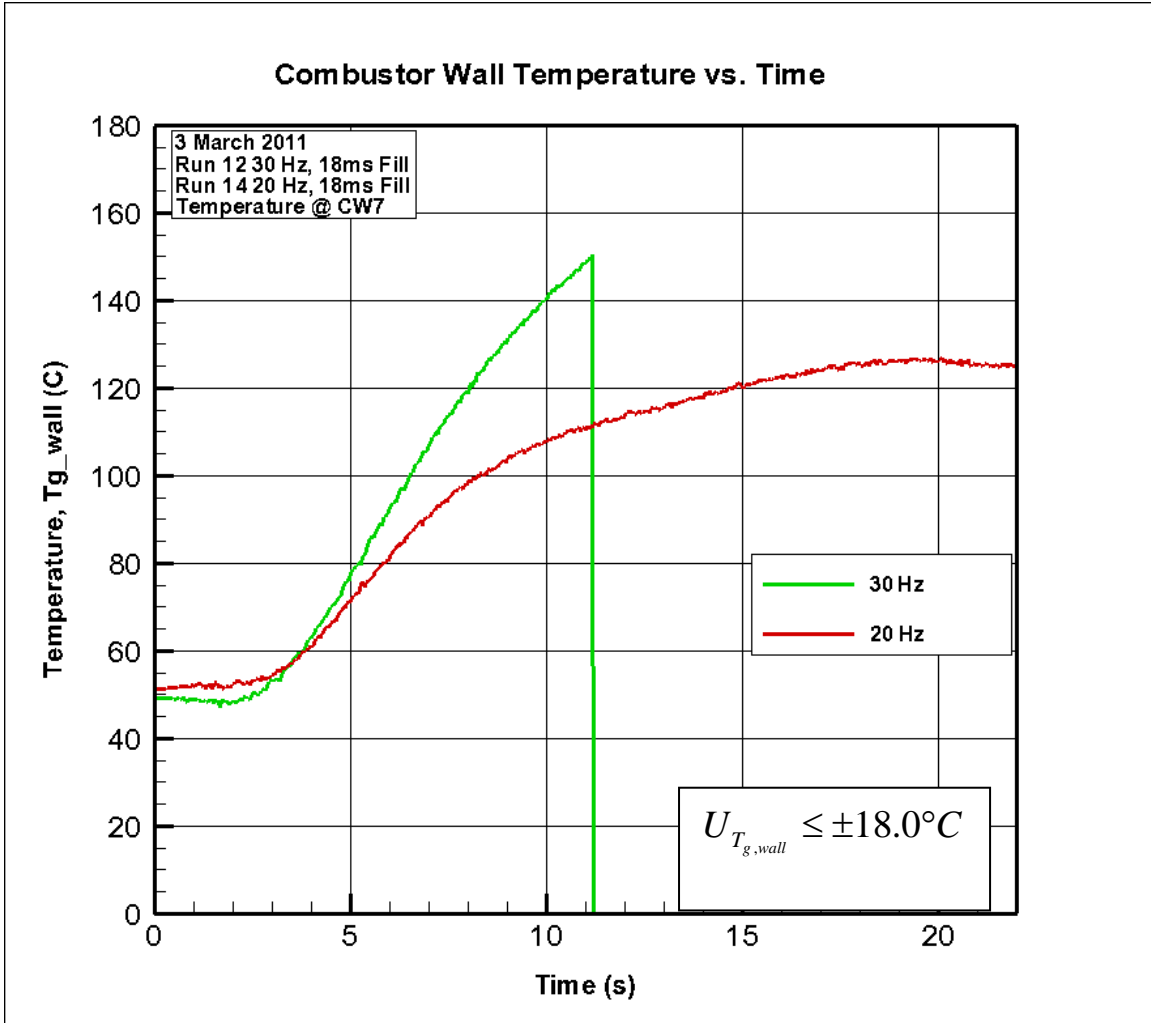


Figure 32. Combustor Wall Temperature Comparisons at 20 Hz and 30 Hz

The temperature profiles along the length of the combustion chamber were compared at three second intervals for 20 Hz and 30 Hz testing. In Figure 34, the dotted lined lines represent the 30 Hz testing temperatures while the solid lines are for 20 Hz temperatures. The shape of the profiles remains similar for each time step. The graph displays an increasing separation of temperatures from 20 Hz to 30 Hz as the run increases. The 30 Hz temperatures are at least 40% greater than the 20 Hz temperatures.

A test run was conducted without any ignition and only used the vitiator to heat the incoming air into the combustor to allow the initial equilibrium conditions to exits. On Figure 34, the combustor wall temperature from only the vitiator nearly duplicates the initial conditions for the start of the 20 Hz and 30 Hz testing.

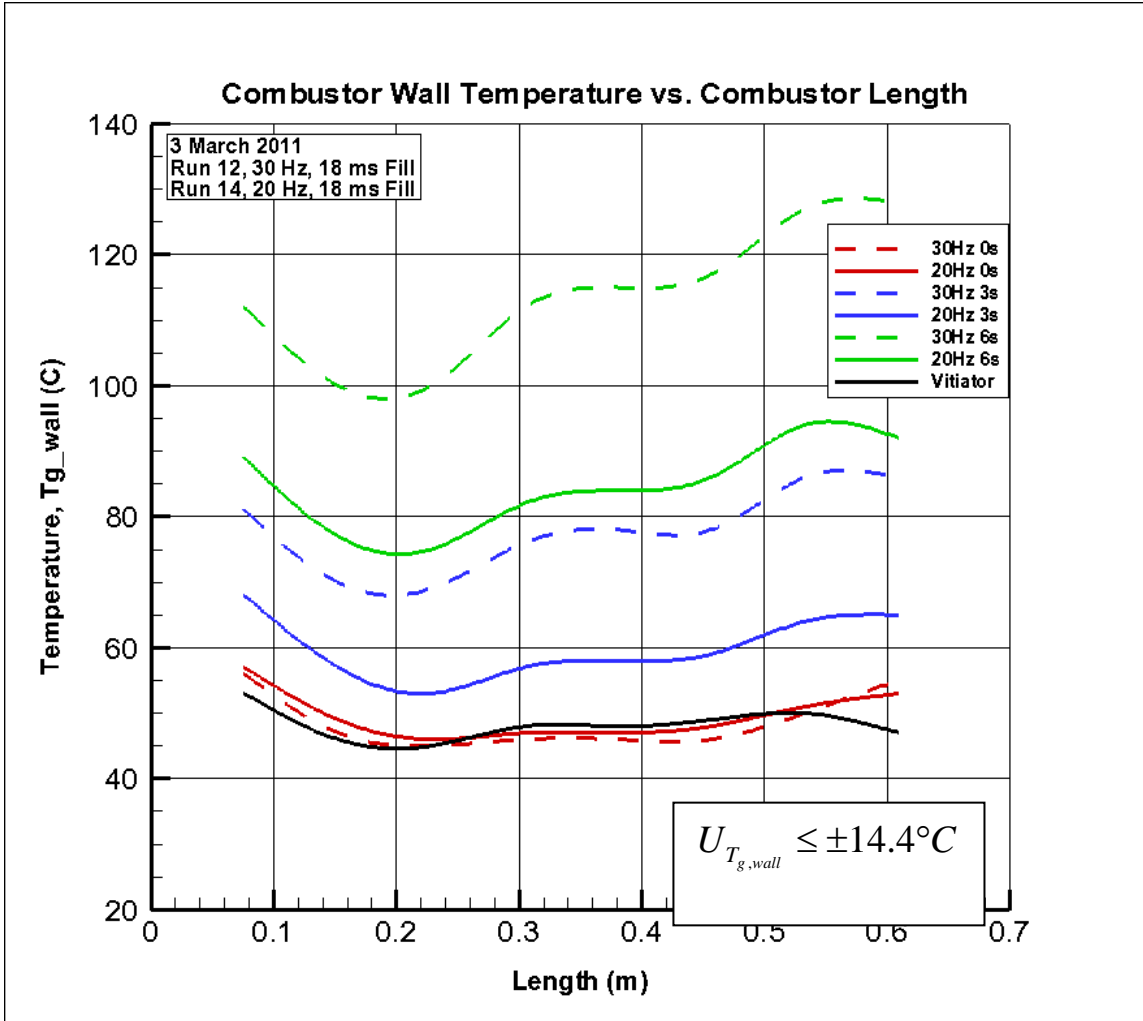


Figure 33. Temperature Profile Comparisons at 20 Hz and 30 Hz

In Figure 35, the heat transfer rates at Cooling Water Jacket 7 are compared for 20 Hz and 30 Hz testing. The 20 Hz heat transfer reached a maximum at about 12 kilowatts at an equilibrium condition. The 30 Hz data was plotted for 10 seconds of operation and then a projected profile was continued to beyond 20 seconds along the same shape. This projected profile produces a maximum heat transfer rate of 18 kilowatts, which is 50%

greater than the maximum for 20 Hz testing. This increase in heat transfer corresponds to a 50% increase in the number of detonations that occurs per second.

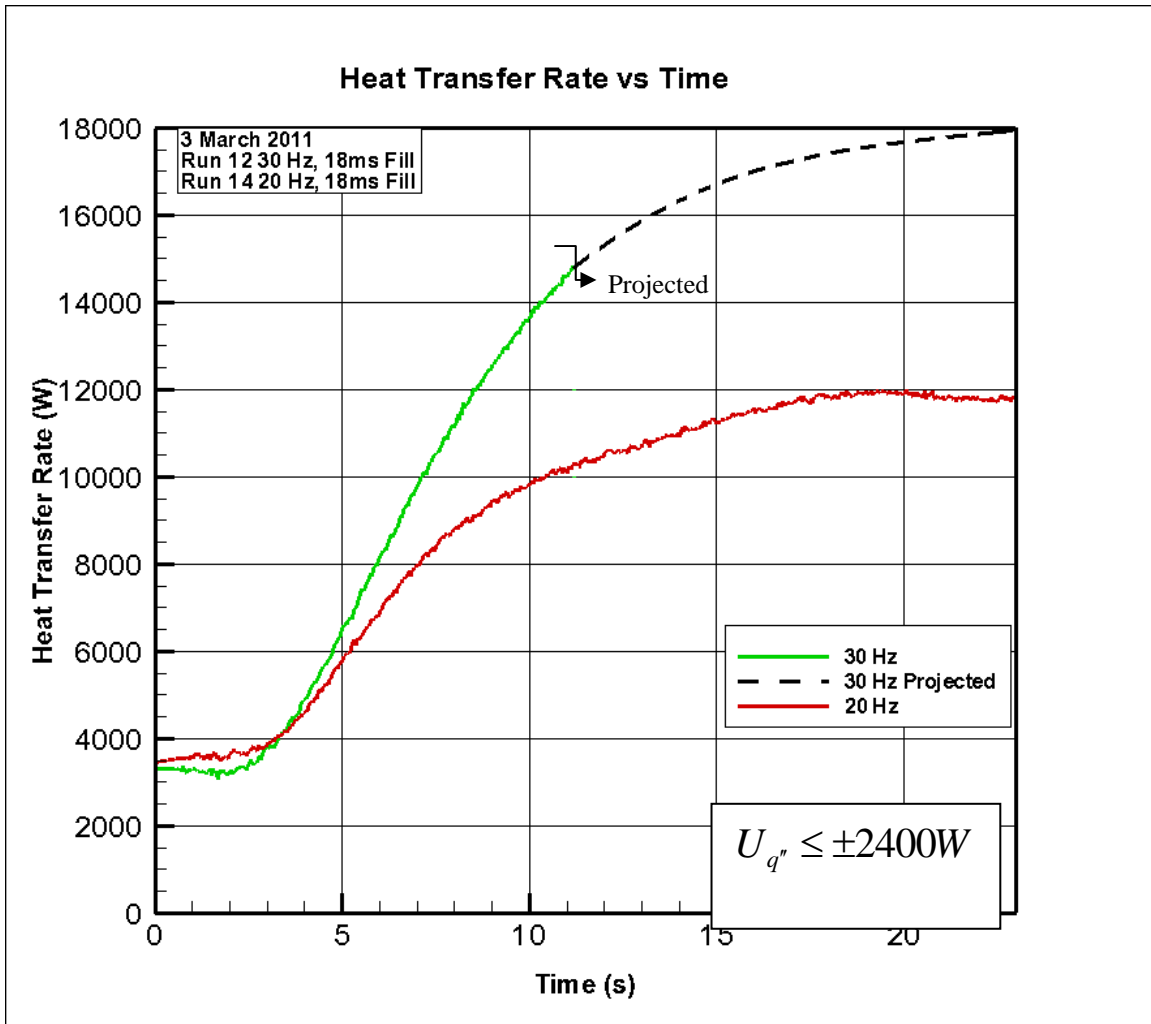


Figure 34. Combustor Wall Temperature Comparisons at CW7 for 20 Hz and 30 Hz

#### D. COMPARISONS OF 30 HZ AND 40 HZ TESTING

Several tests were conducted at 40 Hz and the results were compared to 30 Hz testing. At a frequency of 40 Hz, 33% more detonations occur than during a frequency of 30 Hz resulting in an increased heat transfer rate. The increased frequency resulted in heat transfer rates as high as 16 kilowatts prior to reaching 10 seconds of testing as well as higher inner combustor wall temperatures. Figure 32 displays a comparison of

combustor inner wall temperatures at CW 7 for 30 Hz and 40 Hz testing. It appears that the 40 Hz temperatures are trending about 15% greater than 30 Hz temperatures.

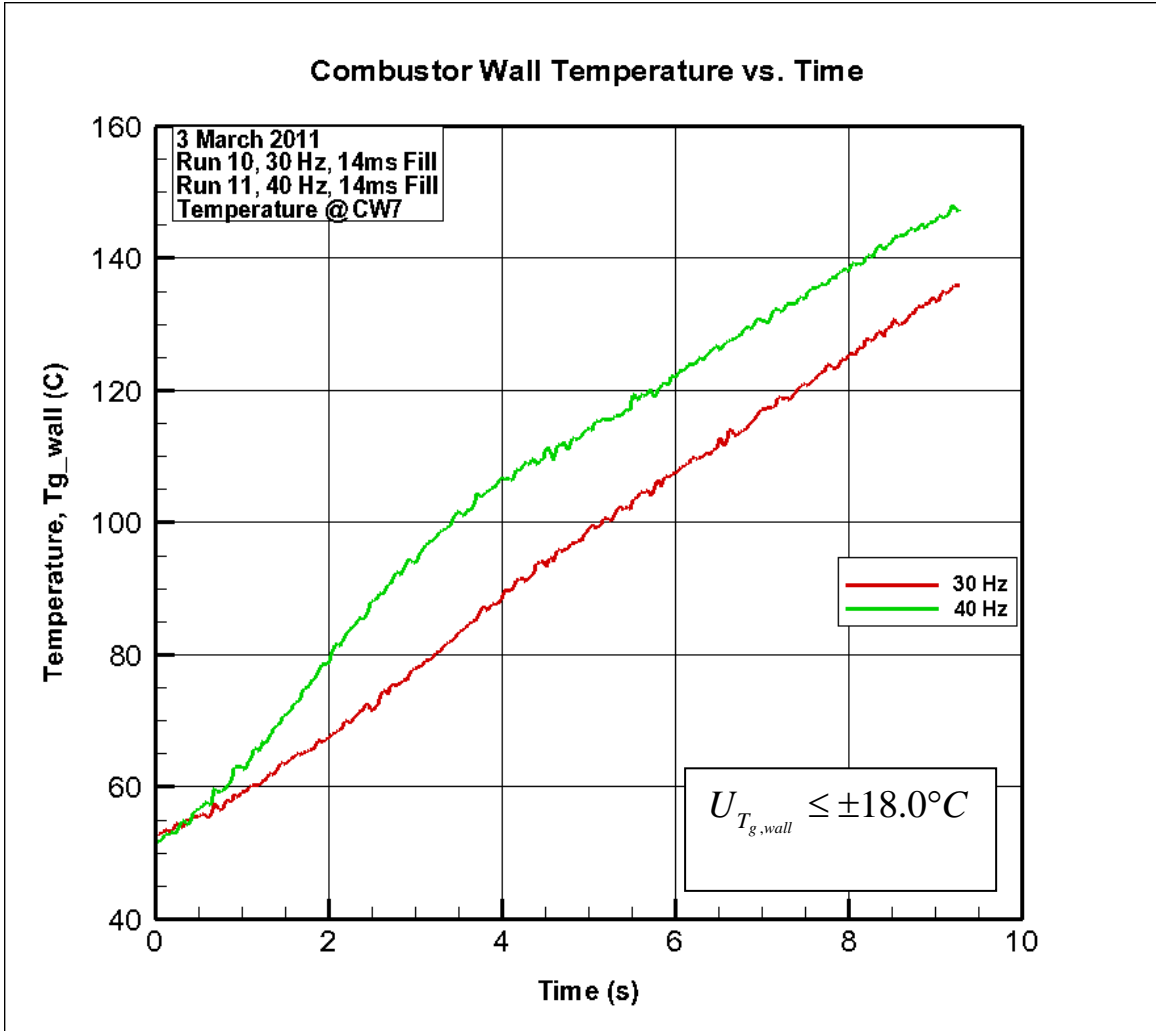


Figure 35. Combustor Wall Temperatures at CW7 for 30 and 40 Hz Tests

## E. COMPUTATIONAL FLUID DYNAMICS MODELING

Computational fluid dynamic modeling was performed using ANSYS CFX software to reproduce the temperature profiles that occur during detonation with an isothermal combustor wall. The CFD was setup for a 0.05 meter diameter combustion chamber without swept ramps using stoichiometric conditions for ethylene gas and air with an initial temperature of 530 K and pressure of 506,625 Pa (5 atm). Figure 36

shows four different time steps during the detonation event in the combustor. The first image is at 250 ms where the detonation wave has just passed point B, about three-quarters the length of the combustor. At point B, the temperatures reached were as high as 3,000 K and close to the Chapman-Jouguet conditions. However, the temperature does not stay this high. As the detonation wave passes, the temperature quickly drops over 600 K in about 0.5 ms as seen in the second image. In the second image, the detonation has reached the nozzle and some shock wave are reflected and heading towards the front of the combustor during the phase known as ring down. The shock wave essentially “resets” the boundary layer conditions. As more time passes, the boundary begins to grow but is still disturbed at 1.5 ms after the initial detonation wave passes. In the last image, the shock waves are further dissipating and the combustor is nearly back to refresh conditions. These conditions are highly transient and make determining a heat transfer coefficient very difficult.



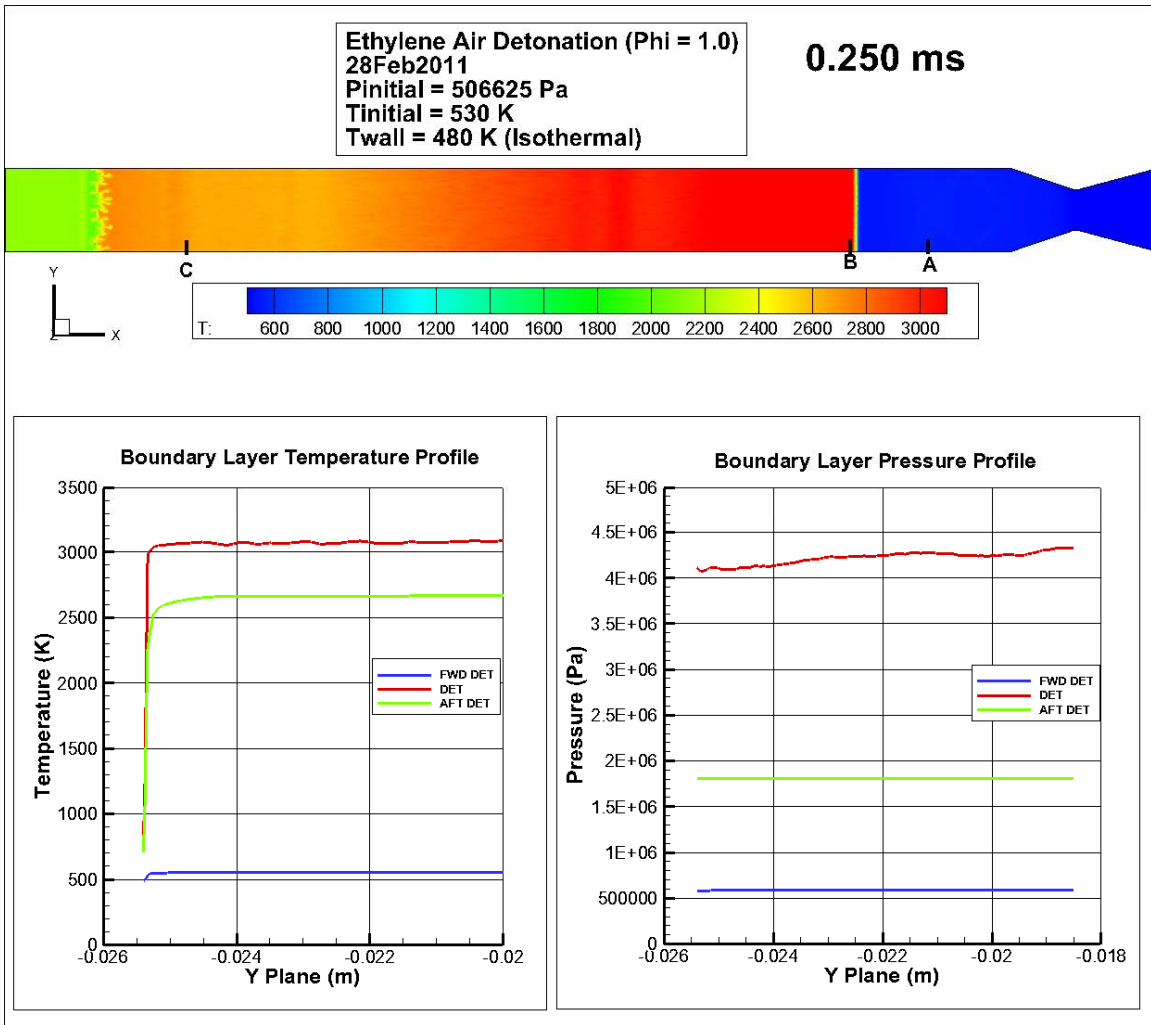


Figure 37. Temperature and Pressure Profile in a Detonation Wave (0.250 ms)

Figures 38 and 39 show the boundary layer temperature profiles at various stages during the ring down event after detonation has occurred. The average bulk flow temperature was determined to be approximately 2,400-2,500 degrees K. This provides about a 2,000 degree K differential temperature from the bulk flow conditions to the combustor inner wall. This increase in thermal and pressure conditions from the detonation are the main driving force of the heat transfer across the combustor wall that occurs for very short time frame of 3–4 milliseconds. After the ring down event occurs, the refresh portion of the cycle begins and the combustion chamber is filled with more air and eventually more fuel.

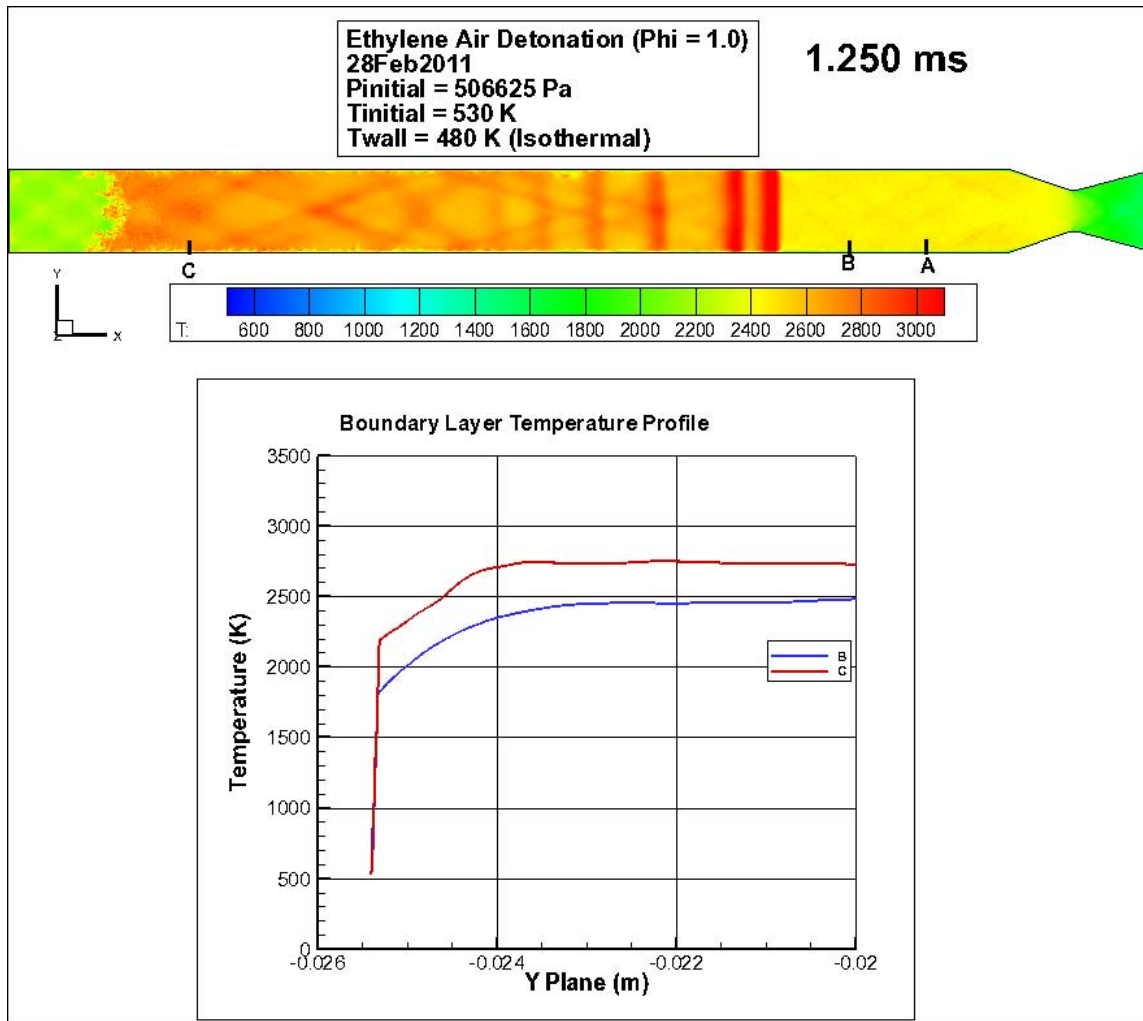


Figure 38. Temperature Profile in a Detonation Wave (1.250 ms)

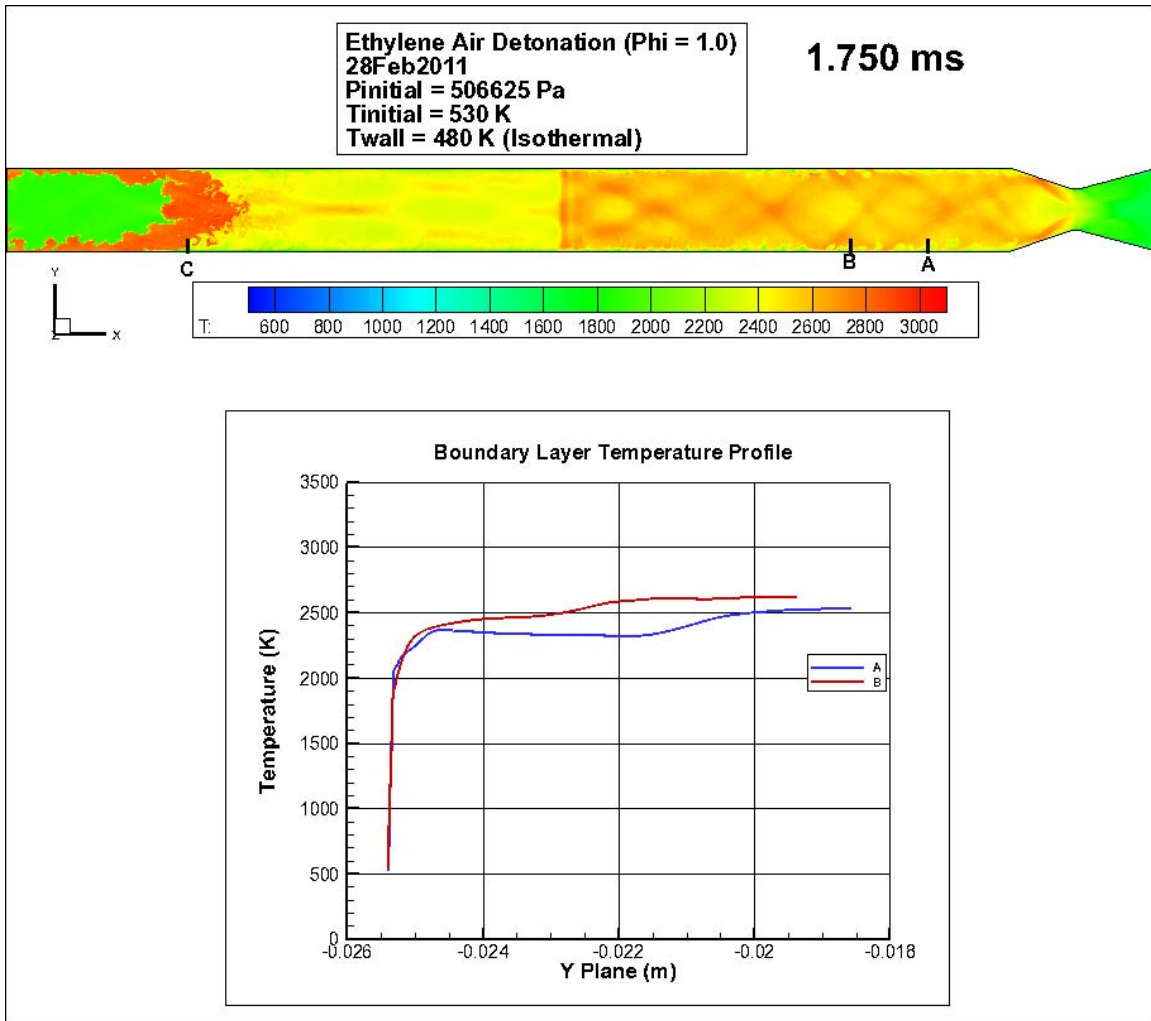


Figure 39. Temperature Profile in a Detonation Wave (1.750 ms)

In order to determine an effective heat transfer coefficient, the detonation event conditions have to be accounted for as well as the refresh conditions. During 30 Hz operation, one cycle occurs every 33.3 ms with the detonation event lasting for approximately 10% of the cycle time. Refresh conditions can be assumed for the remaining cycle time. An average heat transfer coefficient was determined by using the conditions from the CFD and the experimentally measured data from the refresh conditions using the vitiator. For 20 Hz operation, one cycle lasts for 50 ms with 3–4 ms for the detonation event and the remaining time involves purging/filling the combustor with fuel or air. With the maximum heat transfer rate equivalent to 12,000 Watts for 20 Hz steady state testing, one cycle transfers 600 J of energy to a single cooling jacket.

During the refresh conditions, 138 J is delivered based on experimentally determined data. The detonation event must deliver 462 J in 4 ms, resulting in a heat transfer rate of 115,500 W. Using the surface area that the heat transfer occurs across and the differential temperature determined from the CFD, the heat transfer coefficient during detonation would be approximately  $3,166\text{ W}/\text{m}^2\text{ K}$ . This would result in an average in the  $883\text{ W}/\text{m}^2\text{ K}$ . While assuming the maximum heat transfer rate of 18,000 W for 30 Hz testing, the same calculation can be repeated adjusting the cycle time and results in an average heat transfer coefficient of  $1,035\text{ W}/\text{m}^2\text{ K}$ .

It was calculated that each PDC cycle produces almost 300 kilowatts using ethylene at a pressure of 250,000 Pa and a temperature of 400 degrees K, which is similar to operating conditions conducted during testing. Using this information determined that about 1.6% of the energy released during combustion produced was transferred to the cooling water system. This transferred energy could possibly be reused in a regenerative system to preheat the incoming air or fuel.

## **F. UNCERTAINTY ANALYSIS**

An analysis was made to determine the total error associated with equipment accuracies and human error. The type K thermocouples used to measure cooling water temperatures had an accuracy range of  $\pm 2.2^\circ\text{C}$  for temperature below  $293^\circ\text{C}$ . A type K thermometer measured the inlet and outlet temperature, therefore doubling the  $2.2^\circ\text{C}$  possible inaccuracy. A 0.1-second response delay time was used for calculating the error in the mass flow rate measurements. A  $\pm 690$  Pa inaccuracy was assumed for human error of observing the cooling water system differential pressure. These combined inaccuracies and errors resulted in an approximate error of 16.4%, which results in an approximate heat transfer rate of  $11,500\text{ W} \pm 1,900\text{ W}$ . The type K thermocouples accounted for the majority of total error calculated. For future studies, a type T thermocouple should be used with an accuracy of  $\pm 1^\circ\text{C}$ . For an even better result, a Resistance Temperature Detector (RTD) would provide an accuracy of less than  $\pm 0.2^\circ\text{C}$  while operating below  $100^\circ\text{C}$ .

The accuracy of the calculated combustor inner wall temperature was also determined. The Nusselt number was determined from Equation 11, the Dittus-Boelter equation, which may result in errors as large as 25% [7]. A generally more complex equation attributed to Petukhov may reduce the error to less than 10% is shown in Equation 18, which uses the friction factor  $f$ , from the Moody diagram [7].

$$Nu_D = \frac{\left(\frac{f}{8}\right) Re_D Pr}{1.07 + 12.7 \left(\frac{f}{8}\right)^{1/2} (Pr^{2/3} - 1)} \quad (18) \quad (\text{From [7]})$$

The variation in thermal conductivity for 4340 steel was considered negligible for the given operating conditions. An additional  $\pm 2.2^\circ \text{C}$  was added to the mean temperature in Equation 13 for the K type thermocouple. The combined error associated with the heat transfer rate, Nusselt number, and thermocouple resulted in a  $\pm 12.0\%$  total error in the calculated inner combustor wall temperature  $T_{g,wall}$  at steady state 20 Hz operations. The calculated  $T_{g,wall}$  of  $182^\circ \text{C}$  may vary as much as  $\pm 21.9^\circ \text{C}$ . This error could be reduced by using Equation 18 and a more accurate thermocouple.

The effects of natural convection and radiation were calculated for the combustor operating in a  $23^\circ \text{C}$  environment assuming the exterior cooling jacket wall reach equilibrium temperature with the temperature of the cooling water. With assuming an emissivity of 0.85, each cooling jacket section would have an addition 10–20 W, which is negligible considering the orders of magnitude greater heat transfer occurs between the combustor wall and cooling jacket.

THIS PAGE INTENTIONALLY LEFT BLANK

## V. CONCLUSIONS AND FUTURE WORK

### A. CONCLUSIONS

This thesis explored the heat transfer characteristic of a water-cooled PDC through experimental testing and computational analysis. Operational frequencies from 20–40 Hz were considered and found to be directly proportional to the heat transfer rates to the combustor wall. By varying the fill time, or fill fraction, of the fuel from 14–18 milliseconds, the amount of energy transferred along the axis was found to noticeably vary along the combustor.

The cooling water system provided adequate cooling to the combustor wall to allow steady state conditions to be achieved. The amount of cooling necessary to cool to the combustor wall was found to be low enough such that cooling could be achieved by using the air and/or fuel as a cooling medium.

The results from experimental tests revealed that the maximum heat transfer occurs aft of the swept ramp obstacles. The region of increased heat transfer comes as a result from the DDT event occurring just after the last obstacle. This region requires the most amount of cooling and should be considered in future cooling water system designs.

The transient conditions during each detonation cycle created difficulties in obtaining an instantaneous heat transfer rate as well as an instantaneous heat transfer coefficient. By examining the refresh/purge condition separate from the detonation event, an average effective heat transfer coefficient for each portion of the cycle can be approximated providing valuable information towards continuing PDE research. Computer simulations were performed to provide understanding of heat transfer conditions during the detonation wave cycle and allowed for the investigation of the flow field characteristics along the combustor wall as compared to the flow field conditions during detonation and ring down conditions. By combining the experimental research data and the computer simulations, an average heat transfer coefficient could be approximated for different operation frequencies.

## **B. FUTURE WORK**

A redesign of the cooled combustor chamber is currently in progress and will result in a cast mold. A water-cooled combustor with casted swept ramps in the combustion chamber that are cooled as well maximizes the amount cooling to the ramps to help reduce ramp temperatures. By reducing ramp temperatures, the auto ignition of the reactants can possibly be eliminated as being caused by the obstacles in the flow field.

Further research can be conducted using different fuels such as liquid JP-10, which has a higher flashpoint than ethylene/air mixtures. The higher flashpoint could surpass the possible flame-holding event, and allow for longer PDE operation at higher frequencies.

A redesign of the cooling water system as a regenerative heat exchanger using air or fuel would be desirable. A regenerative heat exchange would allow for cooling of the combustor wall while preheating the incoming air or fuel to a higher initial operating temperature. For an air system, a design with a large number of heat exchanger fins might be necessary to provide adequate heat transfer could be determined by heat exchanger effectiveness calculations. A heat exchanger material selection study would provide relevant data to which material can withstand the high frequency mechanical stresses and the associated thermal stresses from detonation while providing adequate heat transfer properties.

# APPENDIX A: PDE STANDARD OPERATING PROCEDURES

## Standard Operating Procedures

### Test Cell #2

Modification Date (27 January 2011)

#### RUN Setup Procedures

1. Lab Personnel – NOTIFY OF IMPENDING TEST
2. Gate – LOCK
3. Red Emergency Stop Buttons (x2) – IN
4. 5V Power Supply – OFF
5. Verify 24V Power Supply (Control Room) – OFF
6. Warning Lights – ON
7. Air Bank Pressure – CHECK >1500 psi
8. Run Sheet – COMPLETE
  - a) Required pressures – NOTE
9. On TC#3 Computer (32-bit)
  - a) “TC2 PDE Control 24 Jan” – OPEN & RUN
    - i. Change data file name, right click data file, select “Data Operations”, select “Make Current File Default”, File – SAVE
  - b) “PDE High Speed 30 July” – OPEN & RUN
    - i. Change data file name, right click data file, select “Data Operations”, select “Make Current File Default”, File – SAVE
10. On TC#2 Computer (32-bit)
  - a) “National Instruments Lab View” – OPEN
  - b) “Test Cell #2.lvproject” – OPEN
  - c) Maximize tree by clicking + symbol
  - d) “Test Cell #2 with Brady Revamp” – OPEN & RUN
  - e) Enter Values from Run Sheet
  - f) “Set Engine Parameters” – SELECT
11. BNC Cabinet Power Strip – ON
12. BNC Box (on top of cabinet) – ON
  - a) CH. A (0.00007 / 0.0) – VERIFY (set with TC#2 computer)
  - b) CH. B (0.00005 / 0.00021) – VERIFY (set with TC#2 computer)

#### Outside

13. Jamesbury Valve – OPEN
14. 24 Volt Power Supply (in TC#0) – ON
15. Node 4 Ball Valve (in TC#1) – OPEN
16. H2 Six Pack 3 Bottle Isolation Valves – OPEN
17. H2 Six Pack 3 Isolation Valve – OPEN & CHECK PRESSURE
18. DAQ Power (in TC#3) – ON
19. Cooling Water System

- a) Test Cell #3 Knife Switch – ON
  - b) Knife Switch Breaker Handle – ON
  - c) Water Tank – CHECK (full and clean)
  - d) Water Tank Isolation Valve – OPEN
  - e) Test Cell #2 Ball Valve – OPEN (ensure TC#3 valve closed)
20. At Overhead Boxes (in TC#2)
- a) Power Supply – ON (170 volts)
  - b) TPI – ON
21. Vitiator Spark Plug – DISCONNECT
22. Main Air (yellow handle) – CLOSE
23. Liquid Injector Cooling Water Valve – OPEN
24. Shop Air (red handle) – OPEN (can verify with blue handle)
25. Node 4 Isolation Valve – OPEN
26. Kistler Amps
- a) Power Switch – ON
  - b) Ensure Proper Setting – 0.380mV
  - c) Function Button – OPERATE
27. Transducer TESCOM Power – ON
28. Gas pressure on Node 22 ( $N_2$ ) to appropriate level to prevent excessive venting – SET
29. Pressurized Gases
- a) Ethylene Ball Valve – OPEN
    - i. Check  $C_2H_4$  pressure in accumulator and note if sufficient. If NOT sufficient perform accumulator fill procedures
  - b) Ethylene Ball Valve - CLOSE
  - c)  $H_2$  – OPEN
  - d)  $H_2$  Torch – OPEN
  - e)  $N_2$  Tank – OPEN
30. Shop Air Tank (closet) – CHECK (95-120 psi)

Inside

31. Set Gas Pressures (in control room)
- a) Node 1; Main Air
  - b) Node 4; High Pressure Air
  - c) Node 20; Vitiator  $H_2$
  - d) Node 22;  $C_2H_4$  controlled with  $N_2$ 
    - i. Set to 2x  $C_2H_4$  pressure
32. 24 volt DC – ON
33. BNC Box – RUN

Outside

34. Main Air (yellow handle) – OPEN
35. Vitiator Spark Plug – CONNECT

\*\*\*\*\*TEST CELL DANGER CONDITION\*\*\*\*\*

Run Profile

1. Personnel – HEAD COUNT
2. LabView Programs – MODIFY FILE NAME AS NECESSARY & RUN
3. Golf Course – CLEAR
4. Siren – ON
5. Emergency Stop Buttons (x2) – OUT
6. 5V Power Supply – ON
7. Main Air – ON
8. Test Cell 2 PDE Controller – START SEQUENCE
9. Cooling Water Pump Switch – ON (After 3-way valve operates)
10. Countdown (Beginning with 4 Second Count From After Time Set for Vitiator)
11. Bottom BNC Controller – START
12. PDE High Speed Data Recording – START

After Run

1. Main Air – OFF
2. Cooling Water Pump Switch – OFF
3. Emergency Stop Buttons (x2) – IN
4. 5V Power Supply – OFF
5. Siren – OFF

Run Shutdown Procedure

1. Emergency Stop Buttons (x2) – VERIFY IN
2. 5V Power Supply – VERIFY OFF
3. Set Gas Pressures
  - a. Node 1 – ZERO
  - b. Node 4 – ZERO
  - c. Node 20 – ZERO
  - d. Node 22 – MAINTAIN CURRENT VALUE (consider minor reduction)
4. BNC Box – OFF
5. BNC Cabinet Power Strip – OFF
6. 24 volt DC – OFF (check with other test cells prior)
7. Jamesbury Valve – CLOSE
8. 24 Volt Power Supply (in TC#0) – ON
9. Node 4 Ball Valve (in TC#1) – CLOSE
10. Vitiator Spark Plug – DISCONNECT
11. Main Air (yellow handle) – CLOSE
12. Kistler Amplifiers – OFF
13. At Overhead Boxes (in TC#2)
  - a. TPI – OFF

- b. Power Supply – OFF
- 14. Water Valve – CLOSE
- 15. Shop Air (red handle) – CLOSE
- 16. Bleed Shop Air (blue handle) – OPEN then CLOSE
- 17. Node 4 Isolation Valve – CLOSE
- 18. Transducer TESCO Power – OFF
- 19. Pressurized Tanks
  - a. H<sub>2</sub> – CLOSE
  - b. H<sub>2</sub> Torch – CLOSE
  - c. N<sub>2</sub> – CLOSE
- 20. Cooling Water Pump
  - a. Test Cell #2 Ball Valve – CLOSED
  - b. Water Tank Isolation Valve – CLOSED
  - c. Knife Switch Breaker Handle – OFF
  - d. Test Cell #3 Knife Switch – OFF
- 21. DAQ Power (in TC#3) – OFF
- 22. H<sub>2</sub> Six Pack – CLOSE & RECORD PRESSURES
- 23. Warning Lights – OFF

## APPENDIX B: COOLING WATER SYSTEM

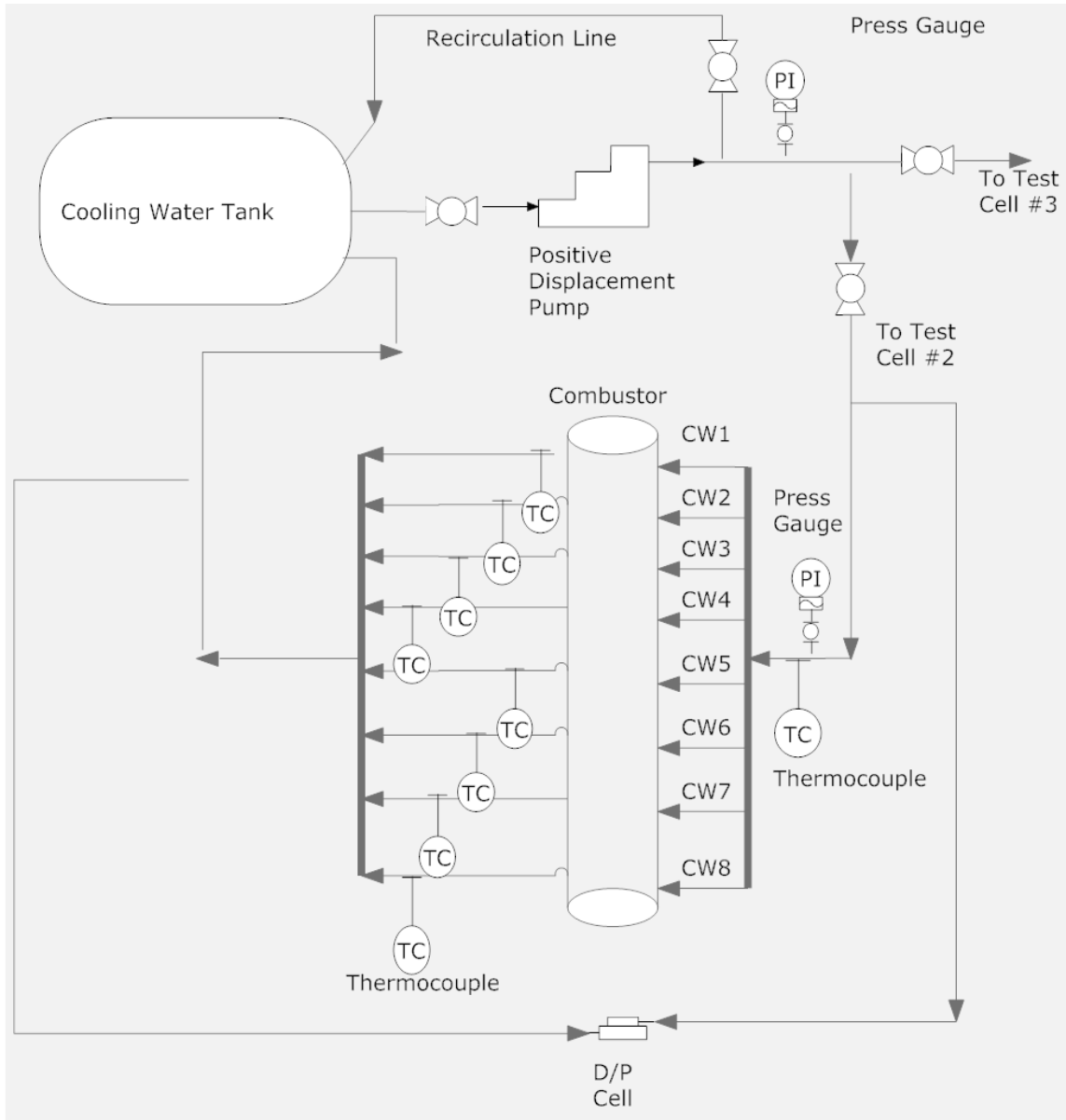


Figure 40. Cooling Water System Schematic

THIS PAGE INTENTIONALLY LEFT BLANK

## APPENDIX C: COMBUSTOR ASSEMBLY DRAWINGS

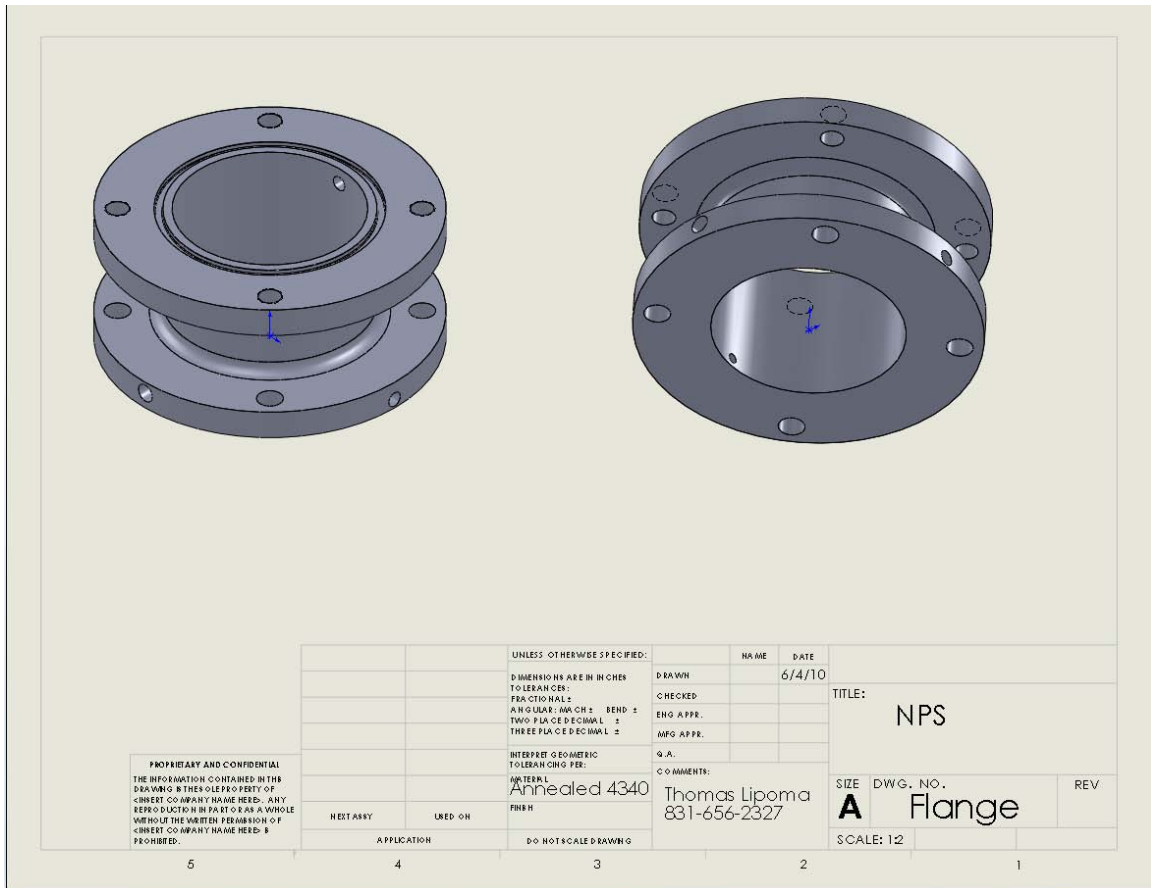


Figure 41. Combustor Section – Isometric View (From [8])

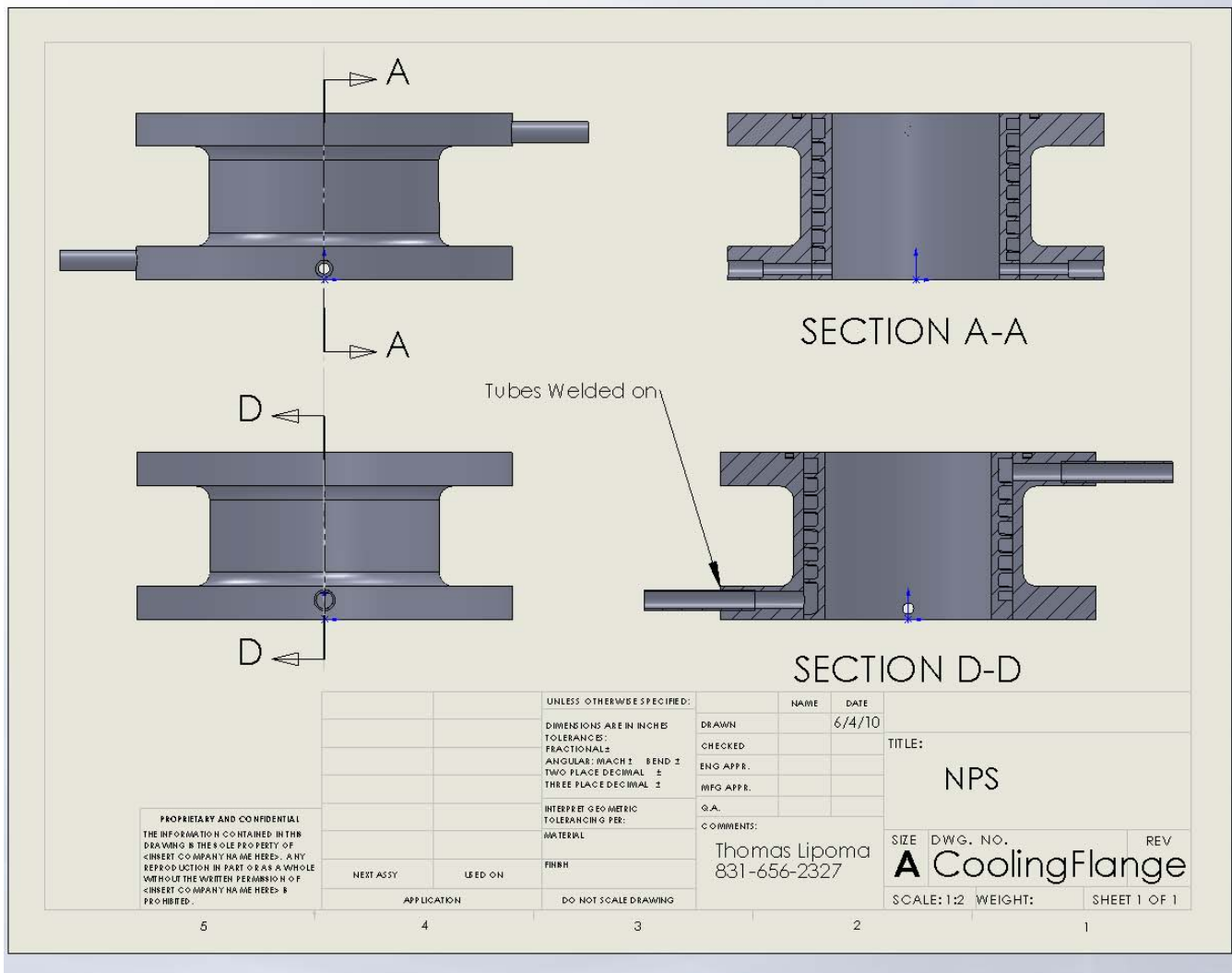


Figure 42. Combustor Sections – Plan View (From [8])

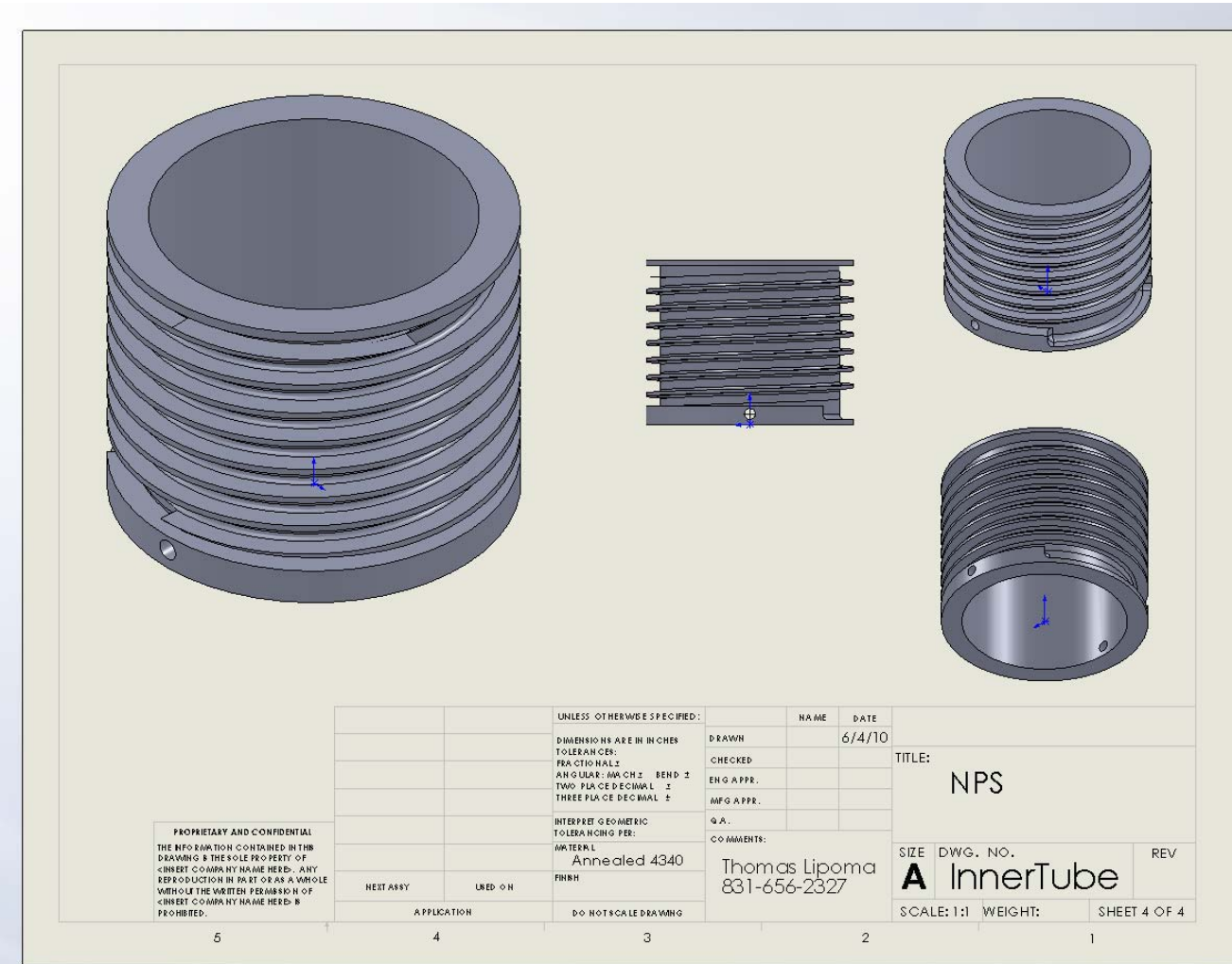


Figure 43. Combustor Sections – Inner Tube (From [8])



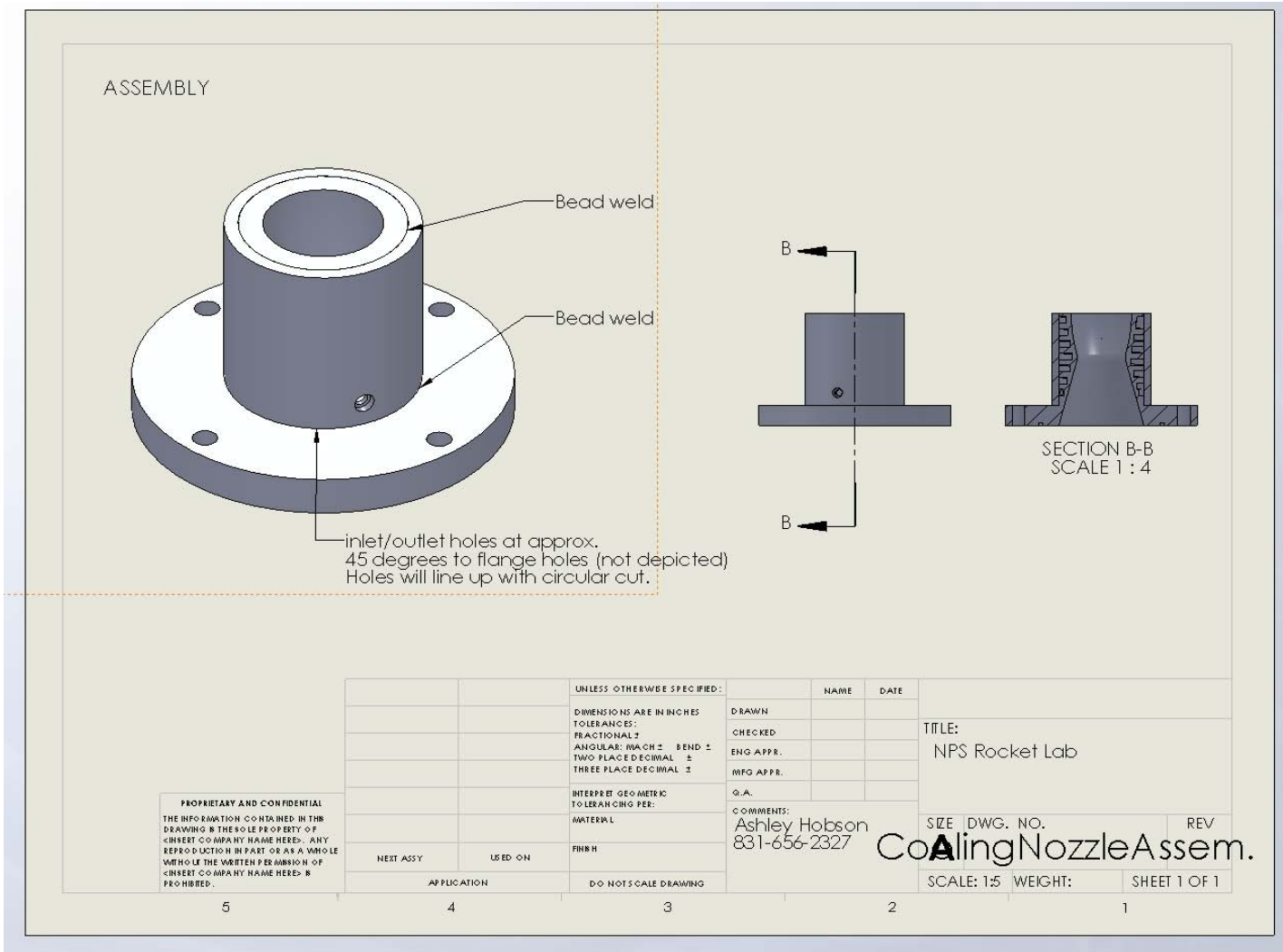


Figure 45. Cooling Nozzle – Assembly (From [8])

THIS PAGE INTENTIONALLY LEFT BLANK

## LIST OF REFERENCES

- [1] R. Friedman, "American Rocket Society," Vol. 24, p.349, November 1953.
- [2] A. G. Naples, J. L. Hoke, and F. R. Schauer, "Study of Heat Loads from Steady Deflagration and Pulse Detonation Combustion," AIAA paper 2010-956, January 2010.
- [3] D. E. Paxson, A. G. Naples, J. L. Hoke, and F. R. Schauer, "Numerical Analysis of a Pulse Detonation Cross Flow Heat Load Experiment," AIAA paper 2011-584, January 2011.
- [4] Aviation Week. <http://www.aviationweek.com/aw/blogs/defense>
- [5] P. D. Hutcheson, C. M. Brophy, and J. O. Sinbaldi, "Investigation of Flow Field Properties on Detonation Initiation" AIAA Paper 2006-5099, *Joint Propulsion Conference and Exhibit*, Sacramento, CA, July 2006.
- [6] W. T. Dvorak, "Performance Characterization of Swept Ramp Obstacle Fields in Pulse Detonation Applications," M.S. Thesis, Naval Postgraduate School, Monterey, CA, March 2010.
- [7] F.P. Incropera, and D.P. Dewitt, *Fundamentals of Heat and Mass Transfer*. New York, N.Y: John Wiley and Sons, 2002.
- [8] D. A. Nichols, "Swept-Ramp Detonation Initiation Performance in a High-Pressure Pulse Detonation Combustor," M.S. Thesis, Naval Postgraduate School, Monterey, CA, December 2010.
- [9] S. H. P. Goh, "Numerical Study of the Effect of the Fuel Film on Heat Transfer in a Rocket Engine Combustion Chamber," M.S. Thesis, Naval Postgraduate School, Monterey, CA, December 2003.

THIS PAGE INTENTIONALLY LEFT BLANK

## INITIAL DISTRIBUTION LIST

1. Defense Technical Information Center  
Ft. Belvoir, VA
2. Dudley Knox Library  
Naval Postgraduate School  
Monterey, CA
3. Christopher Brophy  
Department of Mechanical and Aerospace Engineering  
Naval Postgraduate School  
Monterey, CA
4. Knox Millsaps  
Chairman, Mechanical and Aerospace Engineering  
Naval Postgraduate School  
Monterey, CA
5. Dan Paxton  
NASA Glenn Research Center  
Cleveland, OH
6. Arthur A. Mabbett, Ph.D., P.E.  
Defense Advanced Research Projects Agency (DARPA)  
Tactical Technology Office (TTO)  
Arlington, VA
7. Aaron Esposito  
CENTRA Technology, Inc  
Arlington, VA